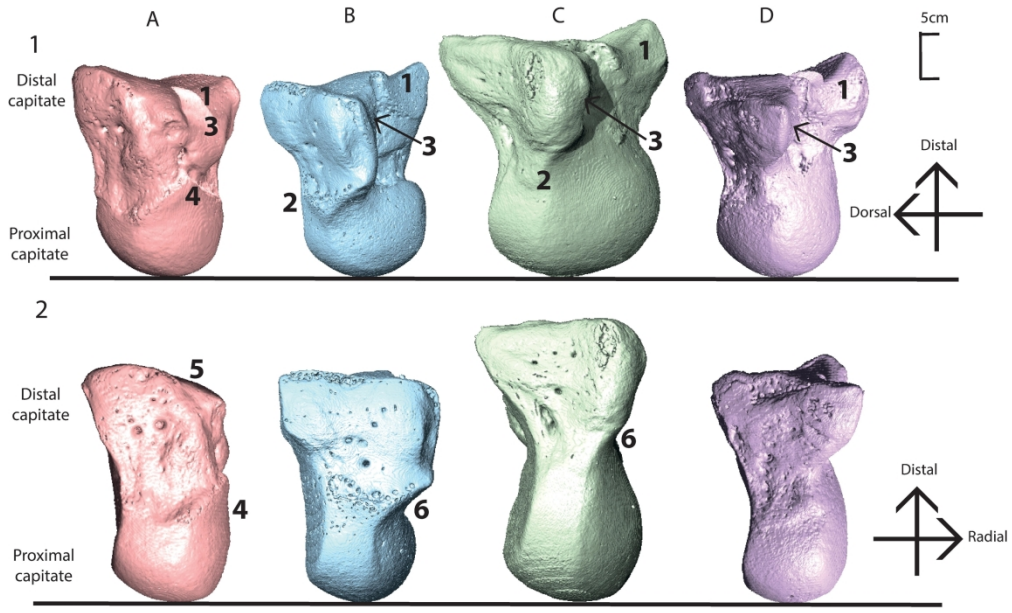

Figure 1. CT-derived surface models of a left capitate from each genus showing variation in external morphology. Capitates have been scaled to relative size. Rows: 1) Capitates are oriented dorso-radially 2) Capitates are oriented dorsally. Columns: A) Homo sapiens (DCW_AM_10_0_182), B) Pan troglodytes (SMF_4104), C) Gorilla gorilla (ZMB_83587), D) Pongo pygmaeus (ZMB_6948). Numbers representing anatomical features: '1' MC2 articulation, '2' Dorsal ridge, '3' trapezoid articulation, '4' radial-palmar expansion of the proximal capitate, '5' MC3 styloid process articulation, '6' waisted mid-capitate.

268x162mm (300 x 300 DPI)

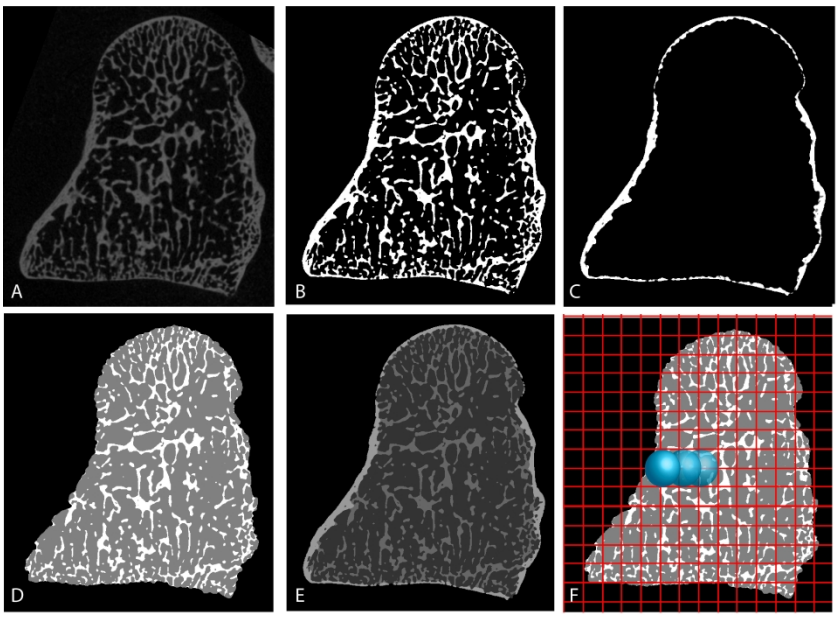

Figure 2. Images showing the morphological filters applied in medtool 4.3 for the whole-bone analysis. A) Original microCT of a Homo sapiens capitate, B) MicroCT scan after MIA-clustering segmentation, C) Cortical thickness image stack, allowing analysis of the cortex only, D) Trabecular bone image stack, allowing analysis of the trabeculae (white) only, E) Combined mask overlay, identifying cortical (lightest grey), trabecular (mid-grey) and air (darkest grey internally and black externally) voxels, F) Sampling sphere (blue) moving across each node of the overlaid 3D grid (red) measuring bone parameters in the trabecular bone image stack.

284x204mm (600 x 600 DPI)

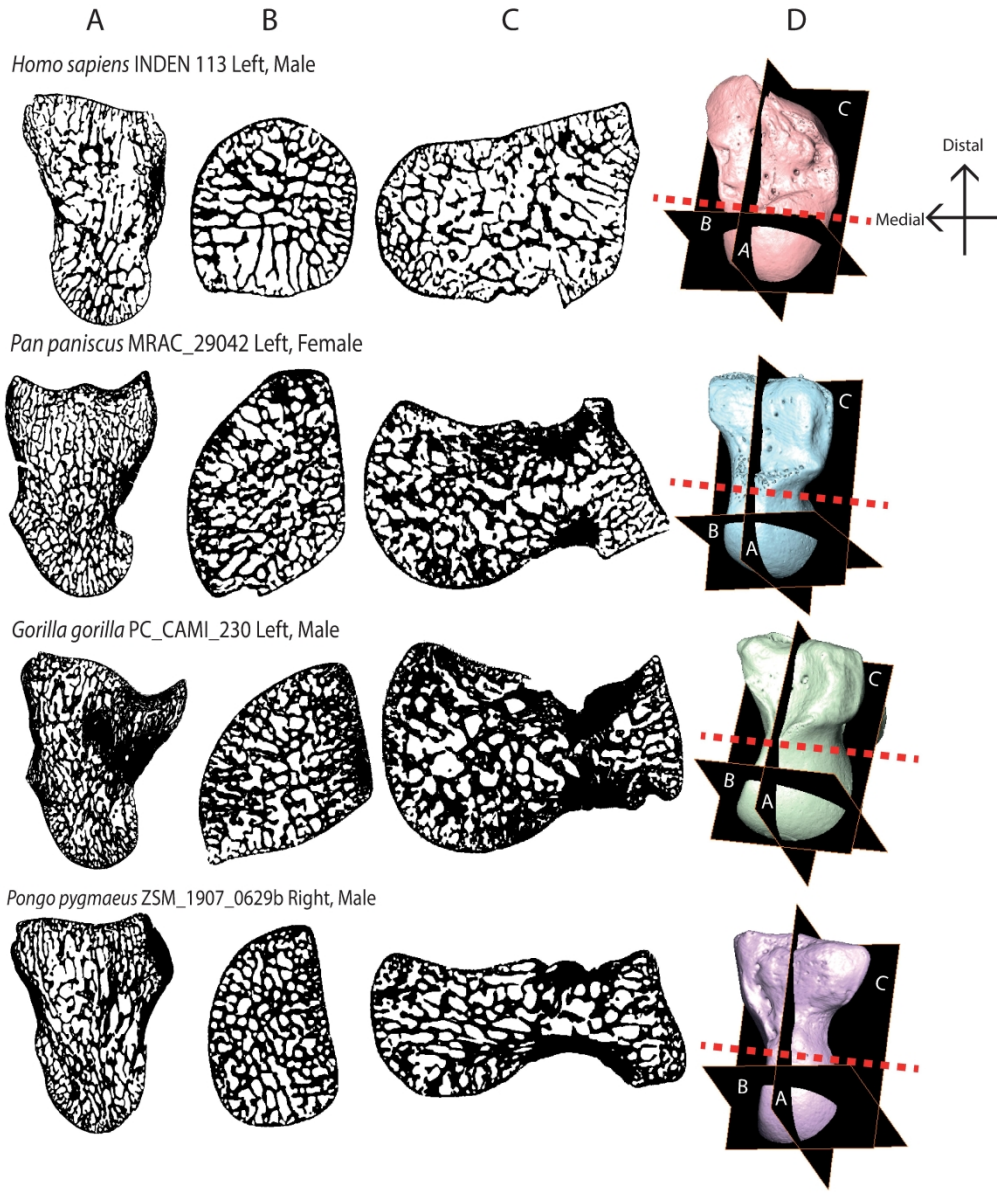

Figure 3. Three cross-sections from the four study genera showing internal bone patterning. A) Y-Z dimension, radial-ulnar cross-section, slice taken from mid-section of bone. Distal is up; dorsal is left. B) X-Y dimension, proximal-distal cross-section, slice taken from proximal mid-capitate. Dorsal is up; radial is left. C) X-Z dimension, dorsal-palmar cross-section, slice taken from midsection of bone. Ulnar is up; proximal is left. D) Surface models of each bone showing the location of cross-section A, B and C. The red dotted line indicates where capitates were partitioned into a distal and proximal portion. Capitates are not to scale. Left capitates have been mirrored.

203x240mm (600 x 600 DPI)

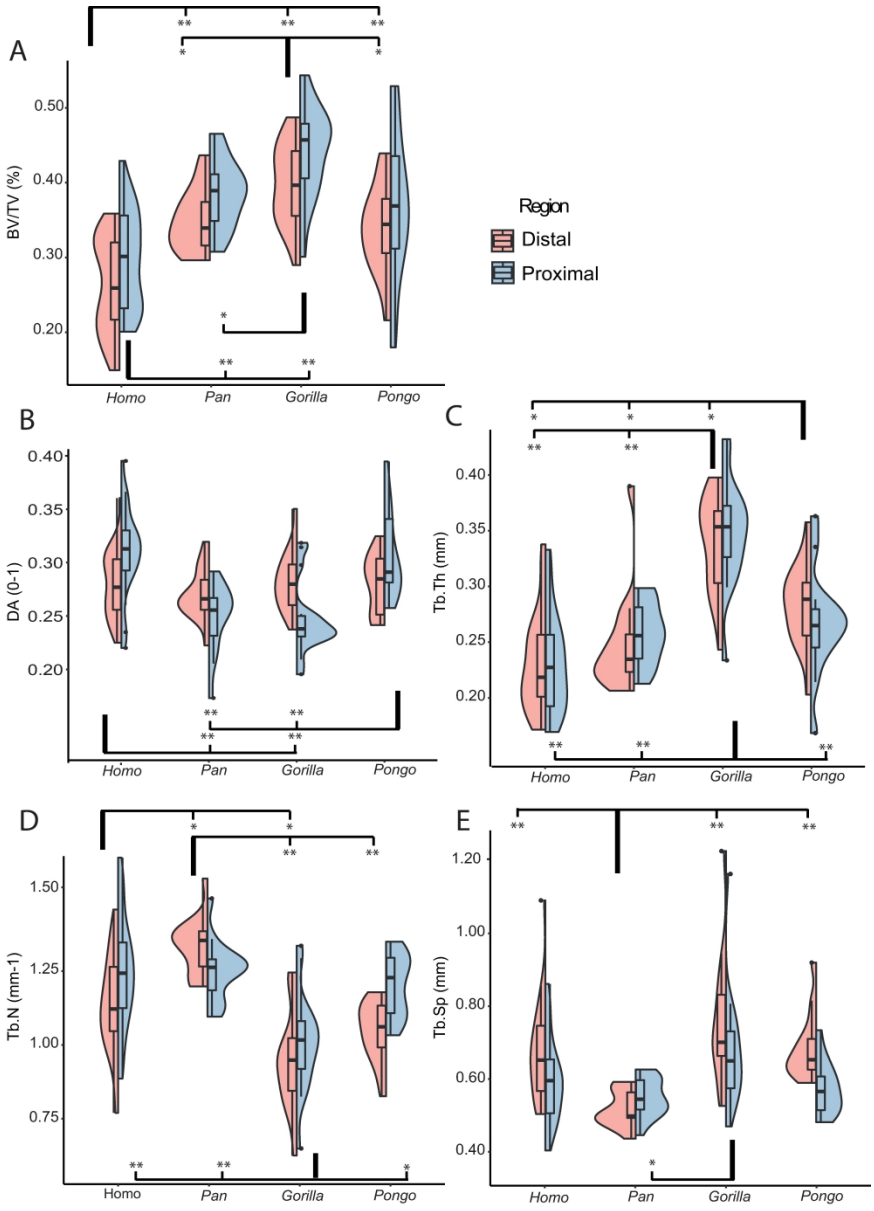

Figure 4. Split violin plots showing the distribution of trabecular results in the proximal and distal segments of each genus. Images are generated using ggplot2 in R (v. 1.2.1335) and utilize the default (Gaussian) kernel density estimation. Colored contours indicate the density of results across the data range. A) Trabecular bone volume to total volume; B) Degree of anisotropy; C) trabecular thickness; D) trabecular number; E) trabecular separation. Outliers are identified with • and represent values 1.5 times above the fourth or below the first interquartile range. For all plots: significant pairwise comparisons are indicated by the square brackets for the distal tests (top of graph) and proximal tests (bottom of graph), * = $p \leq 0.05$; ** = $p \leq 0.001$.

189x262mm (600 x 600 DPI)

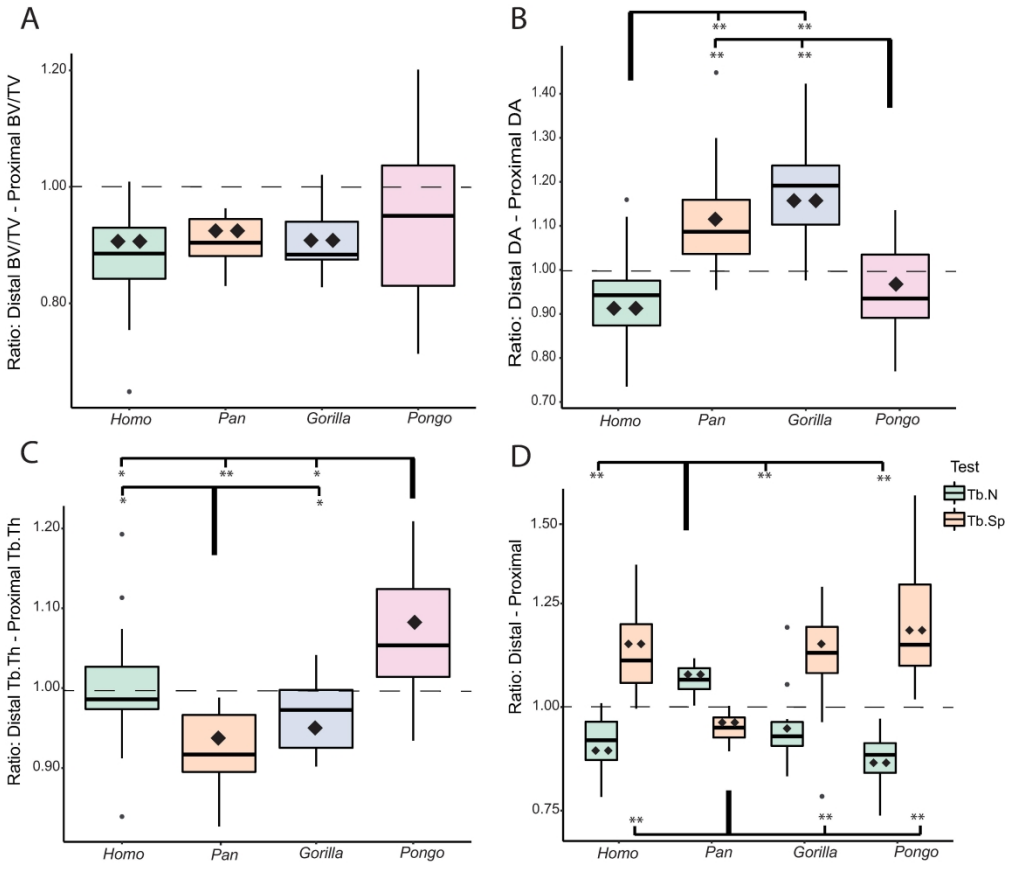

Figure 5. Boxplots of the five trabecular ratios for each genus as well as results for the intraspecific Wilcoxon signed-rank test and interspecific pairwise rank-sum tests. A) Ratio of distal to proximal trabecular BV/TV; B) Ratio of distal to proximal DA; C) Ratio of distal to proximal Tb.Th.; D) Ratio of distal to proximal Tb.N (green) and Tb.Sp (orange). For all figures: Values above the dotted line (ratio = 1) indicate greater trabecular variable in the distal capitate. Significant pairwise comparisons of the ratios are indicated by the square brackets. For D, the top brackets indicate the tests for Tb.N and the bottom brackets indicate those for Tb.Sp. * = p ≤ 0.05; ** = p ≤ 0.001. Significant intraspecific Wilcoxon signed-rank tests between the proximal and distal means are represented by the ♦ symbol thus indicate whether the difference between the mean distal and proximal trabecular variable was significantly different. ♦ = p ≤ 0.05; ♦♦ = p ≤ 0.001.

205x176mm (600 x 600 DPI)

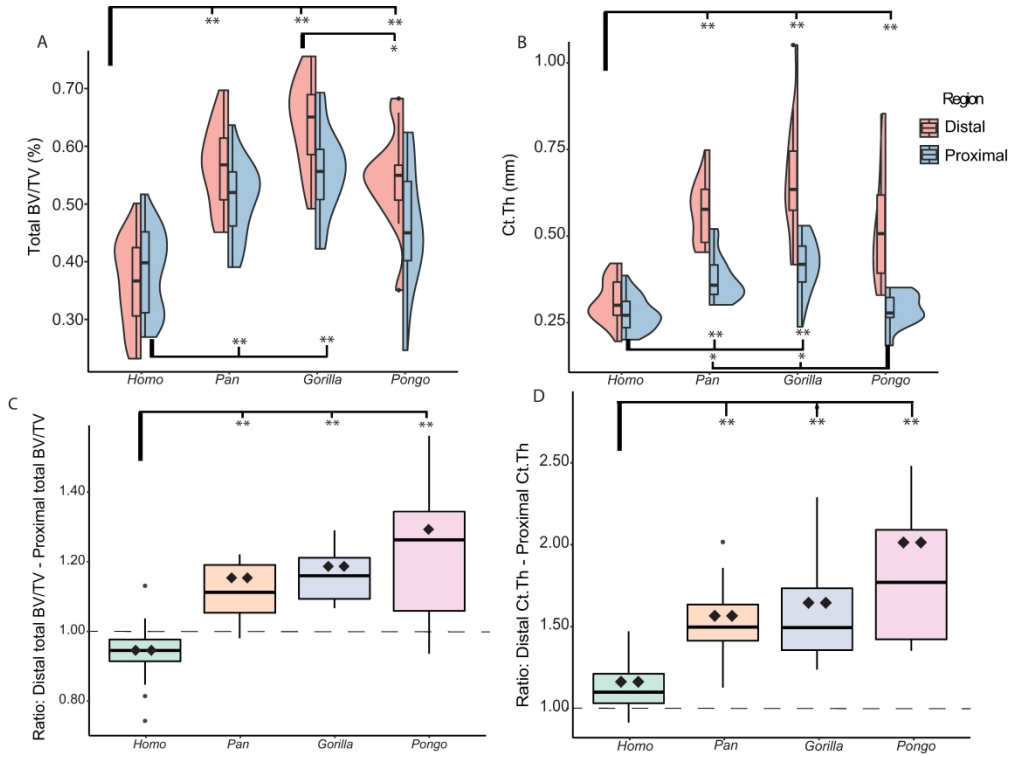

Figure 6. A-B: Split violin plots showing the distribution of total BV/TV (A) and Ct.Th (B) results in the proximal and distal portion of each genus. Images are generated using ggplot2 in R (v. 1.2.1335) and utilize the default (Gaussian) kernel density estimation. Colored contours indicate the density of results across the data range. Outliers are identified with • and represent values 1.5 times above the fourth or below the first interquartile range. Significant pairwise comparisons are indicated by the square brackets for the distal tests (top of graph) and proximal tests (bottom of graph), * = p ≤ 0.05; ** = p ≤ 0.001. C-D: Boxplots showing the distribution of the distal to proximal ratios of the total BV/TV (C) and Ct.Th (D) of each genus. Boxplots also show the results of the intraspecific Wilcoxon signed-rank test and interspecific pairwise rank-sum tests. Values above the dotted line (ratio = 1) indicate greater cortical variable in the distal capitate. Significant pairwise comparisons of the ratios are indicated by the square brackets, * = p ≤ 0.05; ** = p ≤ 0.001. Significant intraspecific Wilcoxon signed-rank tests between the proximal and distal means are represented by the ♦ symbol thus indicate whether the difference between the mean distal and proximal trabecular variable was significantly different. ♦ = p ≤ 0.05; ♦♦ = p ≤ 0.001.

247x185mm (600 x 600 DPI)

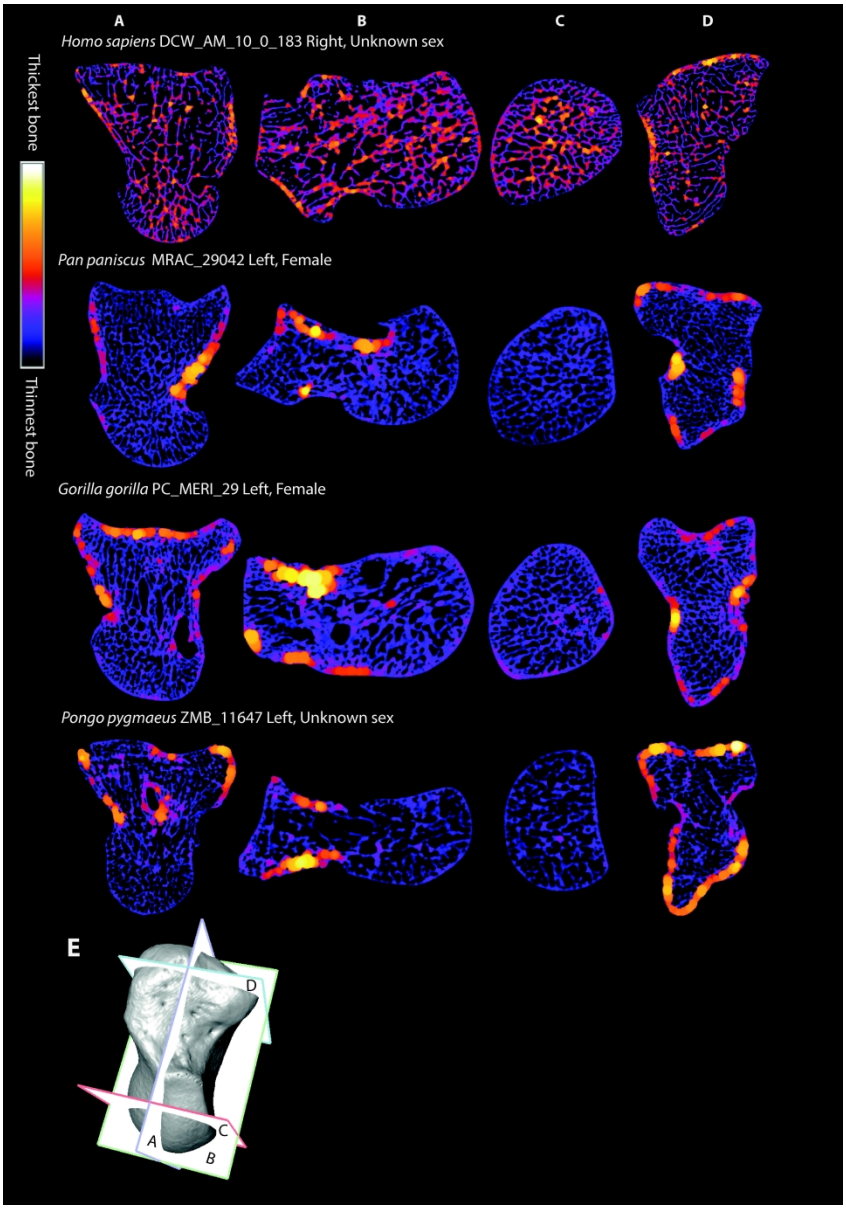

Figure 7. Cross-sections from representative individuals of each genus showing relative trabeculae and cortex thickness across the capitate. A) Y-Z dimension, radio-ulnar cross-section. Distal is up; dorsal is left. B) X-Z dimension, dorsal-palmar cross-section. Ulnar is up; distal is left. C) X-Y dimension, proximal-distal cross-section. Cross-section taken at the proximal mid-capitate. Dorsal is up; radial is left. D) X-Y dimension, proximal-distal cross-section. Cross-section taken at the distal capitate. Dorsal is up; ulnar is left. E) Shows the positions of cross-sections A-D on a Pan specimen. Left capitates have been mirrored. Capitates not to scale.

213x304mm (600 x 600 DPI)

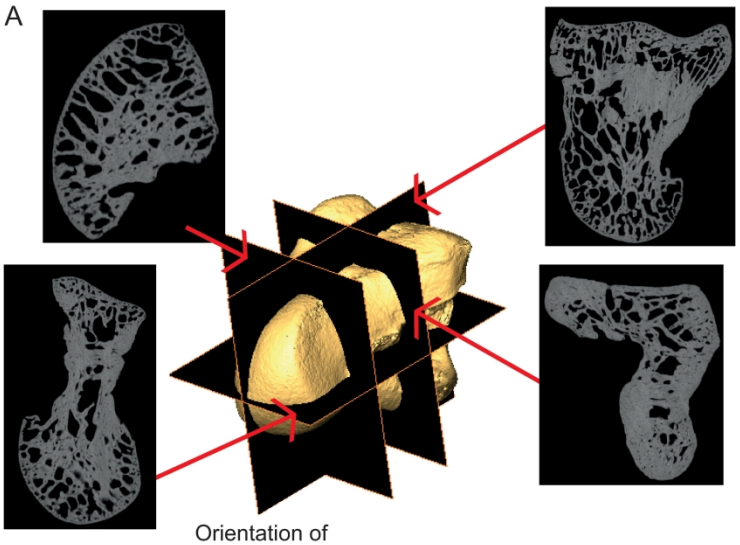

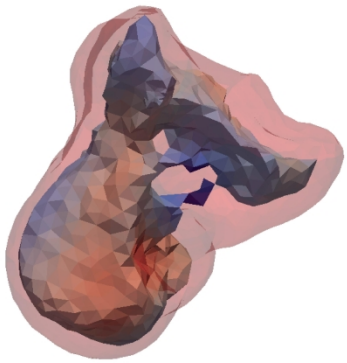

Trabecular BV/TV (%)	
Proximal	0.502
Distal	0.425
DA (0-1)	
Proximal	0.245
Distal	0.280
Tb.Th (mm)	
Proximal	0.378
Distal	0.327
Tb.N (mm^{-1})	
Proximal	1.013
Distal	1.040
Tb.Sp (mm)	
Proximal	0.608
Distal	0.633
Total BV/TV (%)	
Proximal	0.611
Distal	0.718
Ct.Th (mm)	
Proximal	0.327
Distal	0.683

Supplemmentary figure 1: Example of excluded Pan troglodytes specimen, accession ID: PC_ZVII_24, Powell-Cotton Museum. A) CT-derived surface model of Pan capitate showing the location of four cross-sections. Cross-sections show dense and porous bone is continuous throughout the entire capitate. B) Pan specimen visualized after medtool data collection. The whole bone is shown transparent in pink, allowing visualization of the constricted and discontinuous trabecular bone region within. Results of the medtool analysis of this specimen are given in the table.

271x295mm (600 x 600 DPI)

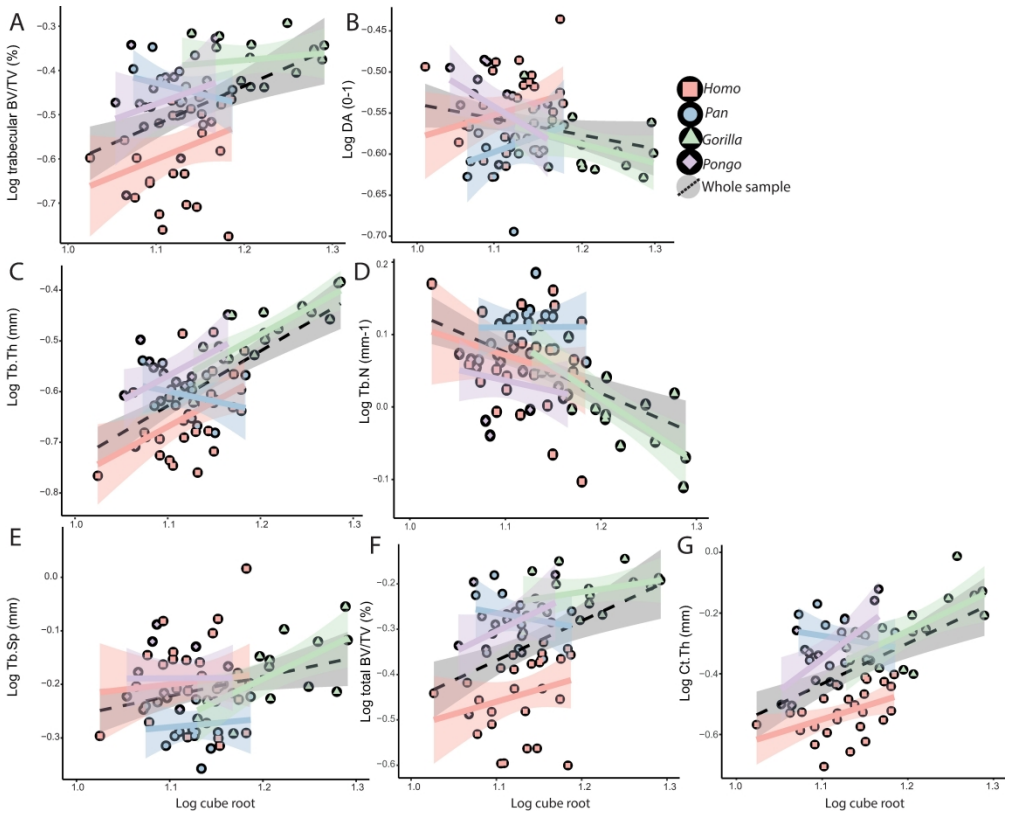

Supplementary figure 2. Plots of the seven RMA regressions testing for allometry. Individual data points are colored by genus and the hominoid trend is indicated by the dotted black line and grey confidence interval. The log cube root of the volume (mm3) is seen across the x axis. A) Trabecular BV/TV; B) DA; C) Tb.Th.; D) Tb.N.; E) Tb.Sp.; E) Total BV/TV; G) Ct.Th.

257x207mm (600 x 600 DPI)

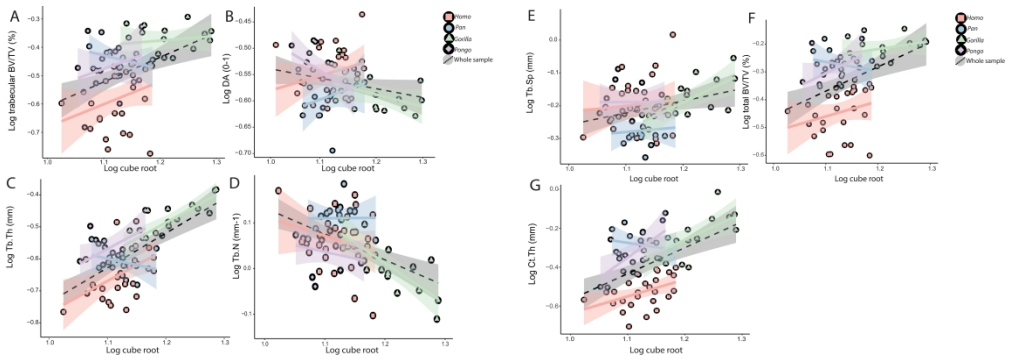

Supplementary figure 2 - large print version. Plots of the seven RMA regressions testing for allometry. Individual data points are colored by genus and the hominoid trend is indicated by the dotted black line and grey confidence interval. The log cube root of the volume (mm3) is seen across the x axis. A) Trabecular BV/TV; B) DA; C) Tb.Th.; D) Tb.N.; E) Tb.Sp.; E) Total BV/TV; G) Ct.Th

589x205mm (300 x 300 DPI)

Cortical and trabecular bone structure of the hominoid capitate

Emma E. Bird[1], Tracy L. Kivell[1, 2], and Matthew M. Skinner[1,2]

[1] Skeletal Biology Research Centre, School of Anthropology and Conservation, University of Kent, Canterbury, UK

[2] Department of Human Evolution, Max Planck Institute for Evolutionary Anthropology, Leipzig, Germany

Corresponding author:

Emma E. Bird

School of Anthropology and Conservation

University of Kent

Marlowe Building

Canterbury, UK, CT2 7NR

Abstract

Morphological variation in the hominoid capitate has been linked to differences in habitual locomotor activity due to its importance in movement and load transfer at the mid-carpal joint proximally and carpometacarpal joints distally. While the shape of bones and their articulations are linked to joint mobility, the internal structure of bones has been shown experimentally to reflect, at least in part, the loading direction and magnitude experienced by the bone. To date, it is uncertain whether locomotor differences among hominoids are reflected in the bone microarchitecture of the capitate. Here, we apply a whole-bone methodology to quantify the cortical and trabecular architecture (separately and combined) of the capitate across bipedal (modern *Homo sapiens)*, knuckle-walking (*Pan paniscus, Pan troglodytes, Gorilla* sp.*),* and suspensory (*Pongo* sp.) hominoids (n=69). It is hypothesized that variation in bone microarchitecture will differentiate these locomotor groups, reflecting differences in habitual postures and presumed loading force and direction. Additionally, it is hypothesized that trabecular and cortical architecture in the proximal and distal regions, as a result of being part of mechanically divergent joints proximally and distally, will differ across these portions of the capitate. Results indicate that the capitate of knuckle-walking and suspensory hominoids is differentiated from bipedal *Homo* primarily by significantly thicker distal cortical bone. Knuckle-walking taxa are further differentiated from suspensory and bipedal taxa by more isotropic trabeculae in the proximal capitate.

In all taxa, bone parameters across the two capitate regions consistently differ, suggesting a variable loading environment between the proximal and distal regions. An allometric analysis indicates that size is not a significant determinate of bone variation across hominoids, although sexual dimorphism may influence some parameters within *Gorilla*. Results suggest that partitioning the capitate (and possibly other short bones) into biomechanically meaningful segments may provide more informative functional analyses for future research. Additionally, while separating trabecular and cortical bone is normal protocol of current whole-bone methodologies, this study shows that when applied to carpals, removing or studying the cortical bone separately potentially obfuscates functionally relevant signals in bone structure.

Key words: locomotion, cancellous bone, functional morphology, primates, wrist

Introduction

Primates use their hands in a diverse set of postures to manipulate and navigate their environment (Fragaszy & Crast, 2016). The many articulations within the wrist are central to the capacity of the hand to move through multiple planes of space and, in combination with soft tissue morphology, joint congruence determines the degree of stability, flexibility and dexterity within the wrist and hand (Orr, 2010). The capitate articulates proximally with the scaphoid and lunate and distally with the trapezoid, hamate, and metacarpals 2, 3 and, sometimes, 4 (Kivell et al. 2016a). As such, the external morphology of the capitate plays a key role in the range of motion at the wrist as it is a central component of the mid-carpal joint proximally and the carpometacarpal joints distally (Jenkins & Fleagle, 1975; Lewis, 1989; Jouffroy & Medina, 2002; Crisco, 2005; Kijima & Viegas, 2009; Orr et al. 2010; Orr, 2017).

The external morphology of the hominoid capitate has featured in hypotheses about the locomotor behavior in the last common ancestor of *Pan* and Hominini (Dainton & Macho, 1999; Richmond et al. 2001; Begun, 2004; Tocheri et al. 2007; Kivell & Schmitt, 2009) and the evolution of hominin dexterity and tool-related behaviors (Marzke, 1983; Niewoehner et al. 1997; Wolfe et al. 2006; Rein & Harvati, 2013). However, drawing locomotor or postural inferences based on external morphology is potentially confounded by the retention of primitive features that are no longer functionally significant (Lieberman, 1997; Ward, 2002; Pontzer et al. 2006; Ruff et al. 2006; Zeininger et al. 2011; Kivell, 2016b). Furthermore, making biomechanical inferences from external morphology requires in-depth knowledge of the form-function relationship of the bone as well as its surrounding soft tissue and articular environment. This is a particular challenge for carpal research as understanding the kinematics and kinetics of the wrist is inherently difficult due to complications in imaging and analyzing the small, closely compacted bones without disrupting the normal kinematic chain (Wolfe et al. 2000; Wolfe et al. 2006; Brainerd et al. 2010; Gatesy et al. 2010; Orr, 2016). While advances in 3D imaging

and computational techniques have begun to improve our knowledge of human wrist biomechanics (see Orr, 2016 for review), our understanding of non-human ape biomechanics remains more limited (but see Orr, 2017 and 2018). Moreover, the functional relationship between cortical and trabecular tissue within short bones is not well understood and it is not clear how they may interact to provide whole bone functionality under the high mechanical loads of locomotion and manipulation. To date, it has yet to be determined whether the internal bone structure of the capitate might reflect differences in hand and wrist use across extant hominoids. Here we apply a whole-bone methodology to investigate how the internal cortical and trabecular bone structure potentially varies within the capitate in a broad sample of *Homo* (recent humans), *Gorilla*, *Pan* (chimpanzees and bonobos) and *Pongo* (orangutans).

Trabecular bone: the relationship between behavior and structure

In addition to some important clade specific synapomorphies (Sarmiento, 1988; Lewis, 1989; Tocheri et al. 2008), the wrists of extant hominoids are adapted to their specialized behaviors and are habitually loaded in different ways. The *Homo* hand is conspicuous among the ape clade as the only species not to habitually utilize the hand for locomotion. Instead, the wrist experiences forces generated predominantly during tool use and other forms of manipulation. High compressive loads are imposed across the wrist by muscle contractions arising from the strong and forceful human thumb as well as flexion of the fingers (Napier, 1956; Marzke 1997; Tocheri, 2007; Marzke, 2009; Bardo et al. 2018). Bones must also withstand and transmit sheer and tensional strains as force is transferred radio-ulnarly across the wrist (Tocheri, 2007; Marzke, 2013). There is an abundance of clinical evidence to support the hypothesis that the Dart Throwers Motion (DTM) is the functional axis of human wrist movement (Crisco et al. 2005; Crisco et al. 2011; Schuind et al. 2013; Brigstocke et al. 2014). The DTM runs from radial deviation in extension to ulnar deviation in flexion and is used across numerous activities from throwing an object to pouring water from a jug (Brigstocke et al. 2014). During this movement, the capitate is very mobile against a stabilized proximal row, with the rotation axis perpendicular to the wrist movement (Crisco et al. 2005).

In contrast, non-human apes utilize their forelimbs during locomotion. *Pongo* utilize a range of torso orthograde suspensory and climbing postures in an almost exclusively arboreal environment (Thorpe & Crompton, 2006; Thorpe & Crompton, 2009; Manduell et al. 2011). In these positions, the wrist experiences substantial tensile loading from gravitational forces and stabilising ligaments, as well as compressive stress from muscle contractions (Swartz et al. 1989; Isler & Thorpe, 2003). *Gorilla* and *Pan* are primarily terrestrial knuckle-walkers, but also engage in various types and frequencies of arboreal locomotion depending on the species, population or sex (van Lawick-Goodall, 1968; Hunt,

1992; Doran, 1993; Remis, 1995; Remis, 1998; Neufuss et al. 2017; Thompson et al. 2018). During knuckle-walking, the wrist must resist compressive loading from both muscle contractions stabilizing the joints and gravitation forces acting on the body mass (Carlson & Patel, 2006). However, the knuckle-walking posture differs somewhat between the two genera. When compared to *Gorilla*, *Pan* typically use more variable hand and forelimb postures, do not bear weight as evenly across the digits and more frequently engage a palm-in forelimb posture (Inouye, 1994; Wunderlich & Jungers, 2009; Matarazzo, 2013; Finestone et al. 2018). *Gorilla* typically knuckle-walk on digits 2-5 and more regularly utilize a palm-backwards forelimb posture (Tuttle, 1969; Inouye, 1994; Matarazzo, 2013), although hand postures in the wild are more variable (Thompson et al. 2018). Although *Gorilla* are hypothesised to use a more neutral, columnar wrist posture than *Pan* (Kivell & Schmitt, 2009), recent kinematic studies of captive African apes found that *Gorilla* and *Pan* were generally similar in their degree of wrist of extension during knuckle-walking (Finestone et al. 2018; Thompson et al. 2020).

Bone functional adaptation describes the biological process of bone altering its structure to optimize resistance against peak mechanical loads habitually experienced throughout the lifetime of the individual (Martin et al. 1998; Ruff et al. 2006; Barak et al. 2011; Doube et al. 2011). Numerous experimental studies suggest that variation in structure reflects, at least in part, load experienced during life (see Kivell, 2016b for review) and thus provides an opportunity to draw behavioral inferences better linked to actual, rather than potential, behavior (Frost, 1987; Ruff & Runestad, 1992). Bone functional adaptation research can not only facilitate a greater understanding of the joint loading and kinematics of extant species but may also provide an informative avenue for behavioral reconstruction in fossil taxa (Griffin et al. 2010; DeSilva & Devlin, 2012; Skinner et al. 2015; Su & Carlson, 2017; Kivell et al. 2018; Dunmore et al. 2020; Georgiou et al. 2020). Previous studies of primate trabecular bone structure within the capitate have used a volume of interest (VOI) sampling sphere but have found limited functional correlation with locomotor behavior (Schilling et al. 2014; Ragni, 2020). However, using a whole epiphysis/bone methodology has been more functionally informative for hand bone studies (Tsegai et al. 2013; Stephens et al. 2016; Tsegai et al. 2017; Stephens et al. 2018; Dunmore et al. 2019; Dunmore et al. 2020). Furthermore, a whole-bone approach to carpal functional adaptation is preferable given their irregular shapes and variation across different taxa (Tsegai et al. 2013; Gross et al. 2014; Schilling et al. 2014).

However, inferring a form-function relationship between bone microarchitecture and behavior is not always straightforward due to several potentially confounding variables (for a comprehensive review and discussion see Kivell 2016b). Firstly, bone modelling (*sensu* Barak 2019) is influenced by the genetic blueprint of the individual, as well as life history factors such as lactation or pregnancy (Kalkwarf & Specker, 1995; Lieberman, 1996; Parsons et al. 1997; Lovejoy et al. 2003; Pettersson et al.

2010; Yeni et al. 2011; Paternoster et al. 2013; Tsegai et al. 2017). Systemic features such as these potentially undermine our ability to differentiate between functional and non-functional patterns expressed in bone structure across different individuals or species. Secondly, there is a higher capacity for functional adaptation to occur during the juvenile and young adult periods and the extent to which bone microarchitectural patterns can be linked to adult behavior has been debated (Bertram and Schwartz, 1991; Pearson & Lieberman, 2004; Ruff et al. 2006). This is particularly salient when analyzing African apes because locomotor behavior is known to differ across age categories (Doran, 1992; Doran, 1997). Finally, there is also uncertainty regarding the loading frequency and magnitude necessary to induce a bone functional adaptation response (Frost, 1987; Ruff et al. 2006; Barak et al. 2011; Wallace et al. 2015). Consequently, microarchitecture will never represent the mechanical ideal of the bone as competing demands on bone tissue will result in a compromise morphology (Ruff et al. 2006).

Cortical bone: contribution to bone structure and functional adaptation

Carpal bones function within an intricate biomechanical environment. The bones and ligaments are interdependent and work together making minor adjustments and movements in concert to create overall hand motion (Lewis, 1989; Kijima & Viegas, 2009; Orr, 2017). Among the carpus, the central role of the capitate within the mid-carpal joint and its articulation with the metacarpus makes it an ideal bone to investigate functional differences in wrist loading. The distal capitate is not only compressed via its carpometacarpal articulations but it also receives tensional strain via the attachment of several extrinsic (between carpals and other hand bones) and intrinsic (between carpal bones) ligaments (Schuind et al. 1995; Kijima & Viegas, 2009; Regal et al. 2020). In contrast, the proximal capitate does not receive any ligaments but forms the 'ball' component of the ball and socket mid-carpal joint within the highly mobile proximal row and is thus loaded predominantly in compression (Lewis, 1989; Garcia-Elias et al. 1994; Kivell, 2016a; Orr, 2017).

Unlike long bones, short bones like carpals generally have a thin cortical shell and the entire internal space is filled with trabeculae (Currey, 2002; Schilling et al. 2014). During movement, short bones are likely to bear a significant portion of the load imposed upon the region as they resist against compressive forces and transfer load through the bone from one joint articulation to another, while also being strained via tensional loads from attached ligaments (Currey, 2002; Yao et al. 2020). Cortical and trabecular bone have divergent material properties due to differences in porosity, mineralization and cellular constitution (Currey, 2002). Cortical bone is stiffer and stronger than trabecular bone (Martin et al. 1998; Guo, 2001), but due to its lower porosity, it is slower than trabecular bone to model and is less compliant (Martin et al. 1998; Hart et al. 2017). While the two tissues work together

to create the functionality of the whole bone, their relative contributions to stiffness, strength and homeostasis differs across regions of the same bone (Doube et al. 2009; Barak et al. 2010). It is not currently understood how cortical and trabecular bone work together to meet the mechanical demands of the carpus, particularly under the high mechanical demands of locomotion.

By quantifying the internal bone architecture of the hominoid capitate using a whole-bone methodology, this study aims to investigate whether differences in trabecular and cortical architecture among hominoids may relate to the divergent hand use across the clade. We also examine the proximal and distal segments of the capitate separately, due to the differences in the soft tissue and articular relationships with the surrounding bones.

Allometry: body size and bone structure

As functional adaptation research aims to identify markers of behavior rather than body size, analyzing bone parameters for allometric effects has been integral to interspecific analyses (Ruff, 1984). Decades of research across various species has yet to find consistent patterns, however some research suggests there may be a general pattern across mammals and birds whereby bone volume to total volume (BV/TV) and degree of anisotropy (DA) are independent of body mass (Cotter et al. 2009; Doube et al. 2011; Barak et al. 2013; Schilling et al. 2014; Christen et al. 2015; Tsegai et al. 2017; Kivell et al. 2018; Komza & Skinner, 2019) while trabecular thickness (Tb.Th), trabecular number (Tb.N) and trabecular separation (Tb.Sp) scale with negative allometry (Barak et al. 2013; Ryan & Shaw, 2013; Kivell et al. 2018; Ragni, 2020). Cortical thickness (Ct.Th) is often reported to be isometric or slightly positively allometric (Runestad, 1997; Demes et al. 2000; Fajardo et al. 2013). However, not all studies find BV/TV and DA to be independent of body mass (for example Fajardo et al. 2013; Ryan & Shaw, 2013; Mielke et al. 2018; Ragni, 2020) nor the negative relationship with Tb.Th, Tb.N and Tb.Sp (for example Doube et al. 2011; Fajardo et al. 2013; Tsegai et al. 2017; Komza & Skinner, 2019.) Few allometric studies have been undertaken on short bones. Tsegai et al. (2017) found no correlation between trabecular parameters or Ct.Th with size in intraspecific analyses of the *Homo* and *Pan* talus. Similarly, an interspecific analysis in Schilling et al. (2014) of the primate capitate found only Tb.N to scale with negative allometry. Ragni (2020) found a greater number of significant relationships within the capitate of *Pan* and *Gorilla* with Tb.Th, Tb.N and Tb.Sp showing negative allometry and DA and BV/TV expressing isometry. These conflicting results may be due in part to methodological differences for sampling trabeculae or calculating size. Nevertheless the effects of allometry on the hominoid capitate remain unclear.

Hominoid capitate morphology

Distal capitate

In all hominoids, the distal capitate is bound to the surrounding bones via strong ligaments which are often described as a unit that moves in unison during extension and flexion (Richmond et al. 2001; Moojen et al. 2003; Crisco et al. 2005; Richmond, 2006; Orr, 2010; Tang et al. 2011). The capitate articulates disto-radially with the trapezoid (although this articulation can be absent in *Gorilla*) and second metacarpal (Mc2), and distally with the third and sometimes fourth metacarpals (Lewis, 1989; Kivell, 2016a). The topology of the metacarpal joint surfaces in the distal row is more complex and irregular in *Pan* and *Gorilla* compared to the smoother surfaces in *Pongo*, however the capacity for extension is linked to the range of movement at the mid-carpal joint rather than at the carpometacarpal junction (Richmond et al. 2001; Begun, 2004; Orr, 2017). The distal capitate in modern *Homo sapiens* is considered to have several derived features linked to committed manipulation and increased efficiency of radio-ulnar force transfer (Tocheri, 2007, Tocheri et al. 2008). A distally-oriented capitate-Mc2 articulation allows pronation of the second finger towards the thumb facilitating precision grip, while a palmarly-positioned and expanded capitate-trapezoid articulation is thought to better resist high radio-ulnarly oriented forces incurred by the thumb during tool-related activities (Marzke, 1997; Tocheri, 2007; Tocheri et al. 2008). Furthermore, the disto-dorso-radial corner is truncated to accommodate the third metacarpal (Mc3) styloid process, providing a stable joint for transmitting high forces and resisting subluxation of the third ray during tool use (Marzke & Marzke, 1987; Riley & Trinkaus, 1989; Niewoehner et al. 1997; Tocheri et al. 2008; Ward et al. 2014). In non-human apes, load transfer also occurs radio-ulnarly as bones of the distal carpal row are compressed against one another. However, in contrast to humans, the orientations of the articular surfaces of the capitate (and distal carpal row more generally) indicate the wrist is better adapted to withstand and transfer proximo-distally oriented forces, which arise during use of the forelimb in locomotion (Tocheri, 2007; Tocheri et al. 2008). Only a small proportion of the dorsal surface of the distal capitate is without articular surfaces. In this distal segment, compression is induced at the distal, radial and ulna articular surfaces, while tension is induced by the supporting intrinsic ligaments surrounding these articulations. Tension further arises from the several intrinsic and extrinsic ligaments attached to the palmar and dorsal surfaces (Kijima & Viegas, 2009; Regal et al. 2020).

Proximal capitate

In great apes, the rounded proximal surface of the capitate articulates with the bones of the proximal row to form the crux of the mid-carpal joint (Kivell 2016b). No ligaments attach directly onto the proximal capitate thus compared to the distal row, the bones of the mid-carpal joint are able to move

more independently of one another (Moojen et al. 2003; Crisco et al. 2005; Kijima & Viegas, 2009; Regal et al. 2020). In *Pongo*, the proximal capitate is radio-ulnarly narrow in comparison to the other great apes (Fig. 1) (Richmond et al. 2001). Notably, the os centrale is not fused to the scaphoid as it is in the other hominids, and thus excludes the scaphoid from articulating with the capitate resulting in relatively greater freedom of movement at the mid-carpal joint (Begun, 2004; Orr, 2018). In *Pan* and *Gorilla*, the proximal capitate is enlarged on the radial aspect, which produces a "waisted" mid-region forming an embrasure with the trapezoid (Richmond et al. 2001; Wolfe et al. 2006; Kivell, 2016a; Orr, 2018). There is also a notable radio-ulnar ridge along the distal extent of the dorsal articular surface that extends onto the hamate (Richmond et al. 2001). These features contribute to the so called "screw-clamp mechanism" that describes the functional complex limiting extension at the mid-carpal joint. During extension, the scaphoid is wedged in between the capitate and trapezoid, providing stability between the proximal and distal row (Tuttle, 1969; Jenkins & Fleagle, 1975; Richmond et al. 2001; Orr, 2005; Richmond, 2006; Orr, 2017). *Homo* also exhibits the fused scaphoid-os centrale and radially expanded proximal capitate, however an enlargement of the bone in the radial-palmar region results in a less dramatic "waisting" of the bone, resulting in a range of extension intermediate between the other hominoids (Lewis, 1977; Lewis, 1989; Orr, 2017). Notably, the proximal capitate is the crux of the functional axis of the DTM (Crisco et al. 2005). During motion, the rotation axis of the capitate is perpendicular to the movement of the DTM as it moves across a virtually motionless scaphoid and lunate (Crisco et al. 2005). Thus, although a small bone, the proximal and distal portion of the capitate functions within notably different ligamentous and articular environments.

[FIGURE 1 ABOUT HERE]

Hypotheses

This research centers on two interrelated hypotheses for both trabecular and cortical bone that are summarized in Table 1 and elaborated below.

[TABLE 1 HERE]

Trabecular bone architecture

We predict that the capitate of knuckle-walking *Gorilla* and *Pan* will have high relative BV/TV and high DA (Table 1, hypothesis 1) due to the presumed high compressive forces and reduced mobility from their more extension-limiting mid-carpal joint. In contrast, we predict that the *Pongo* capitate will have intermediate BV/TV and low DA due to their predominantly suspensory behavior, resulting in reduced compression but greater mobility. We expect *Homo* to exhibit low BV/TV and intermediate

DA because their capitate is not loaded during locomotion and presumably has the least compressive loading but more predictable movement along the DTM axis.

Given the differences in mobility and presumed loading between the proximal and distal portions of the capitate, we hypothesize that there will be differences in the trabecular bone structure between these segments (measured as ratios). It is predicted that the distal aspect will have higher BV/TV and DA compared to the proximal aspect across all species (Table 1, hypothesis 2). As there are no previous studies that have addressed this question for the capitate, we test the null hypothesis that these ratios will be similar among the study taxa. Although we report Tb.Th, Tb.N and Tb.Sp, we do not make explicit predictions about these parameters because all contribute, potentially in a variety of different combinations, to BV/TV.

Cortical bone thickness

The contribution of cortical bone to the functional adaptation of the capitate in hominoids has never been investigated. Given the assumed loading differences described above, we predict that the cortical bone will be thickest in *Gorilla* and *Pan*, followed by *Pongo*, with *Homo* exhibiting the thinnest cortex (Table 1, hypothesis 1). Also following the predictions for trabecular bone, it is predicted that the cortex of the distal capitate should be significantly thicker than the proximal capitate for all genera.

In long bones, the joint surface tends to have a thin layer of cortical bone covering a dense trabecular network that transfers load towards the thicker and stronger diaphyseal cortex (Currey, 2002). In short bones, the cortex is similarly described as thin, however the relationship between cortical and trabecular bone has never been quantified among hominoids. Additionally, it is unclear whether the behavioral differences among ape genera will result in different ratios of cortical to trabecular bone. Therefore this study will investigate the relative contribution of cortical bone to total bone volume, testing the null hypothesis that these ratios will be similar among the study taxa (Table 1, hypothesis 2).

Inter- and intraspecific allometry in internal bone structure

As this study incorporates hominoids of diverse body size, inter- and intraspecific allometry is also investigated. Predictions are outlined in Table 1 (hypothesis 3) and follow the results of Schilling et al. (2014) for the interspecific and Tsegai et al. (2017) for the intraspecific predictions.

Materials and methods

Sample

The study sample includes capitates (n=69) from *Homo sapiens* (n=26), *Pan troglodytes* and *Pan paniscus* (n=14), *Gorilla* sp. (n=16) and *Pongo* sp. (n=13) (Table 2; Supp. Table 1). These taxa are categorized into three behavioral groups based on their most frequent locomotor behaviors: bipedal (*Homo*) knuckle-walking (*Gorilla* and *Pan*) and suspensory (*Pongo*). Capitates from non-human apes were wild-shot adults with no obvious signs of pathology. Consideration was given to ensuring a sex balance for each taxon when possible, however 16 specimens had unknown sex.

[TABLE 2 HERE]

Computed tomography

Capitate specimens were scanned with either a BIR ACTIS 225/300 high-resolution microCT scanner or a Diondo D3 high-resolution microCT scanner at the Department of Human Evolution, Max Planck Institute for Evolutionary Anthropology, Germany, or a Nikon 225/XTH scanner at the Cambridge Biotomography Centre, University of Cambridge, United Kingdom. Specimens were scanned with an acceleration voltage of 100-160 kV and 100-140µA using a 0.2-0.5mm copper or brass filter. Images were reconstructed as 16-bit TIFF stacks. To ensure accurate post-scan segmentation of thin trabeculae, scan resolution was limited to a maximum of 0.048mm (average 0.032mm) for non-human apes, and 0.035mm (average 0.029mm) for the *Homo* sample. This resolution is below the suggested range for minimal error detection (Isaksson et al. 2011; Christen et al. 2016) Post-scanning, each capitate was positioned into approximately the same orientation using Avizo 6.0 (Visualization Sciences Group, SAS). Segmentation of trabecular bone, including identification and removal of extraneous non-bone material, used the medical image analysis (MIA) clustering method (Dunmore et al. 2018). The MIA-clustering method increases the reproducibility of results by reducing subjective input parameters required for other segmentation methods (Dunmore et al. 2018).

Data collection

This study uses the medtool 4.3 software package (http://www.dr-pahr.at/medtool/) to quantify bone parameters throughout the entire capitate utilizing the method outlined in Gross et al. (2014). In brief, medtool utilizes a series of morphological filters to identify the cortical, trabecular, internal (marrow) and background elements of the segmented CT scans. After MIA segmentation, medtool projects a series of rays onto outside of the bone (Fig.2B) that continue to move internally through the bone until a non-bone voxel is reached (Pahr & Zysset, 2009a). By using a value of average trabeculae

thickness, morphological filters fill and close small holes present in the porous cortex allowing a smooth boundary contour between cortical and trabecular bone to be identified (Pahr & Zysset, 2009a; Pahr & Zysset, 2009b; Gross et al. 2014). Two *Gorilla*, one *Pan* and two *Pongo* specimens were excluded from the sample as the internal cortical-trabecular boundary could not be confidently defined due to extreme cortical porosity (an example is provided in Supp. Figure 1). Medtool then superimposes the trabecular-cortical boundary to the original image such that the pores within the cortex are maintained for analysis. Porosity is important to maintain within the cortical bone when quantifying microarchitecture as it has been linked to strength and elastic modulus (see Cooper et al. 2016 for review). Unique scalars are applied to the background, cortical, trabecular and internal elements of the scan. A series of image stacks are created and include a cortex only stack (Fig. 2C), trabecular and internal only stack (Fig. 2D) and a trabecular and cortical combined stack (Fig. 2E). A 3D grid with 2.5mm spaced nodes is then superimposed on an image stack and a 5mm sampling sphere moves from node to node to measure parameters across the entire bone (Fig. 2F) (Pahr & Zysset, 2009a).

BV/TV is calculated as the ratio of bone to non-bone voxels. DA is calculated via the Mean Intercept Length (MIL) method (Whitehouse, 1974) and is calculated as 1 – (min. eigenvalue/max. eigenvalue) which produces a number limited between 1 and 0, with 1 being complete anisotropy and 0 being complete isotropy. Tb.Th, Ct.Th and Tb.Sp are computed in a similar way to the more well-known BoneJ® plugin (Doube et al. 2010) for ImageJ. Spheres are grown within the trabecular or cortical bone and medtool calculates the diameter of the largest sphere that fits within the bone (Hildebrand & Rüegsegger, 1997). For the calculation of Tb.Sp, medtool inverts the greyscale values of the image stack (Fig. 2E) such that the 'internal' voxels are now represented by the 'bone' scalar. Similar to Tb.Th and Ct.Th, spheres are then grown within the internal voxels until a trabecular or cortical voxel is reached. The results of Tb.Sp and Tb.Th are used to calculate Tb.N using the formula 1/(Tb.Th+Tb.Sp).

Cortical and trabecular parameters were quantified in the whole capitate, as well as proximal and distal VOIs. To produce these VOIs, each capitate was cut just distal to the ulnar-most point of the ridge delineating the extent of the lunate articulation on the dorsal proximal capitate, as per the measurement made in Richmond (2006) (Fig. 3D). These VOIs are subjected to the same data collection process as outlined in Fig. 2, quantifying all of the trabecular or trabecular and cortical bone within the proximal or distal segment. This delineation separates the proximal VOI as the section of the bone that does not contain any ligament attachment sites, from the distal VOI which does receive ligamentous attachments. To assess and compare the relative contribution of cortical bone to total bone volume, BV/TV was measured twice: firstly, in only the trabecular region of the bone (Fig. 3D) as determined using medtool (see above) and, secondly, in the original MIA segmented specimen in

which there is no partitioning between cortical and trabecular bone (Fig. 2B). This provides a measure of BV/TV that combines cortical and trabecular bone (referred to as 'total BV/TV' throughout). Relative thickness maps of Ct.Th and Tb.Th are generated by loading the Tb.Th output into ImageJ (1.50b) (https://imagej.nih.gov/ij/) and visualized using the 3D Volume Viewer plugin (http://rsb.info.nih.gov/ij/plugins/volume-viewer.html)

[FIGURE 2 ABOUT HERE]

Statistical analysis

Trabecular bone hypotheses

Mean differences in the proximal and distal trabecular parameters (trabecular BV/TV, DA, Tb.Th, Tb.N, Tb.Sp) were compared interspecifically using a Kruskal-Wallis one-way ANOVA and pairwise Wilcoxon rank-sum tests using the Holm p adjust method (*R* Core Team, stats package v3.6.1) (Table 1). A distal to proximal ratio was calculated for each parameter and a Wilcoxon signed-rank test was applied within-genus to test whether the mean values of the ratio were statistically significant. A Kruskal-Wallis one-way ANOVA and pairwise Wilcoxon rank-sum test examined interspecific differences in the ratios.

Cortical bone hypotheses

To test for differences in cortical bone, mean differences in total BV/TV and Ct.Th were compared interspecifically in the proximal and distal segments using a Kruskal-Wallis one-way ANOVA and pairwise Wilcoxon rank-sum tests using the Holm p adjust method (*R* Core Team, stats package v3.6.1).

Within each genus, a distal to proximal ratio was calculated for each parameter and a Wilcoxon signed-rank test was applied to test whether mean values of the ratio were statistically significant. Additionally, we examined taxonomic differences in these ratios using a Kruskal-Wallis one-way ANOVA and pairwise Wilcoxon rank-sum tests.

Two additional ratios were calculated in order to test for taxonomic differences in the relative proportion of cortical and trabecular bone. These ratios were compared between species, using a Kruskal-Wallis one-way ANOVA and pairwise Wilcoxon rank-sum tests using the Holm p adjust method (*R* Core Team, stats package v3.6.1).

Inter- and intra-specific allometry

To test for allometric trends in the capitate, each whole-bone cortical and trabecular parameter was inter- and intra-specifically analyzed in a reduced major axis regression (RMA). As a proxy for body

mass, the volume (mm^3) of each capitate was calculated in Paraview (4.8.2) using the Integrate Variables filter. The logged cube root of the volume was regressed against the logged bone parameters using the lmodel2 package in *R* (v1.7-3; Legendre, 2018). Interpretation follows Ryan and Shaw (2013); the shape parameters of BV/TV, DA and Tb.N will have an isometric slope equal to 0; values greater than 0 indicate positive allometry while values less than 0 are indicative of negative allometry. Size parameters, such as Ct.Th, Tb.Th and Tb.Sp will have an isometric slope of 1; positive allometry is indicated by a value greater than one and negative allometry by values of less than 1. All statistical tests conducted for hypotheses 1, 2 and 3 are considered significant if $p \leq 0.05$.

Results

Trabecular bone

Cross-sections of each genera in Fig. 3 provide an example of the internal structure of the capitate within three planes of view. The red dotted line in Fig. 3D indicates where the capitate was partitioned into the proximal and distal segments.

Bone volume to total volume

Proximal and distal trabecular BV/TV differ significantly across the study sample (p=<0.001 for both tests, Sup. Table 3). *Gorilla* has the highest proximal and distal BV/TV followed by *Pan*, then *Pongo*, with *Homo* having the lowest BV/TV values (Supplementary Table 2). Proximally, pairwise comparisons show that *Pongo* is not differentiated from any other taxa, while other pairwise comparisons are significant. Distally, all pairwise comparisons are significant except between *Pongo* and *Pan* (Fig. 4A, Sup. Table 3).

Intraspecific comparisons of the BV/TV ratio (distal BV/TV relative to proximal BV/TV) reveal that all genera have greater trabecular BV/TV in the proximal aspect (Fig. 5A, Sup. Table 4, Sup. Table 5). The differences between the two VOIs reach statistical significance in *Homo*, *Pan* and *Gorilla* (p=<0.001 for three tests; Sup. Table 4) but are non-significant in *Pongo*. The Kruskal-Wallis test on the BV/TV ratio reveal that it does not differ significantly among the study sample (p=0.429) indicating that although BV/TV differs between the proximal and distal capitate, the way it differs is similar among the hominoids.

[FIGURE 3 ABOUT HERE]

Degree of anisotropy

Proximal DA differs significantly among the study sample (p=<0.001) however distal DA does not (p=0.593, Sup. Table 3). Notably, DA is the only trabecular parameter which has a different significance result for the proximal and distal VOI. *Homo* and *Pongo* have the highest proximal DA with 0.30 followed by *Pan* and *Gorilla,* both with 0.24 (Fig. 4B, Sup. Table 2). Distal DA differs by only 0.02 between the genera, with the highest value from *Gorilla* at 0.28 and lowest from *Pan* at 0.26 (Sup. Table 2). Pairwise comparisons reveal that proximally, *Homo* and *Pongo* are differentiated from *Pan* and *Gorilla* (p=<0.001 for all four significant tests). Distally, there are no significant pairwise results (Fig. 4B, Sup. Table 3).

Both *Gorilla* and *Pan* have a higher DA in the distal VOI whereas *Homo* and *Pongo* both have higher DA in the proximal and the difference between the proximal and distal VOIs is significant for all genera (Fig. 5B, Sup. Table 4). The DA ratio differs significantly across the genera (p=<0.001) and pairwise comparisons reveal that *Homo* and *Pongo* are differentiated from *Pan* and *Gorilla* (p=<0.001 for all four significant tests, Sup. Table 4).

Trabecular thickness

Tb.Th differs significantly across both the proximal and distal capitate of the study sample (p=<0.001 for both tests, Sup. Table 3). *Gorilla* has the highest mean thickness followed by *Pongo*, with *Homo* having the thinnest (Supp. Table 2). Distally, all pairwise comparisons are significant except between *Homo* and *Pan*. Proximally, *Gorilla* is differentiated from all other taxa (Fig. 4C, Sup. Table 3).

Homo, *Pan* and *Gorilla* have thicker trabeculae in the proximal aspect and *Pongo* in the distal aspect (Sup. Table 4 and 5). The difference between the two segments is statistically significant for *Pan*, *Gorilla* and *Pongo* but not for *Homo* (Fig. 5C, Sup. Table 4). The Tb.Th ratio differs significantly among the study sample (p=<0.001) and all pairwise comparisons are significant except between *Homo* and *Gorilla* (Sup. Table 4).

Trabecular number

Proximal and distal Tb.N differs significantly among the study sample (p=<0.001 for both tests, Sup. Table 3). *Gorilla* has the lowest trabecular number while *Pan* has the highest number (Sup. Table 2). Distally, all pairwise comparisons are significant except between *Pongo* and *Homo*, and *Pongo* and *Gorilla*. Proximally, only *Gorilla* is differentiated from all other taxa (Fig. 4D, Sup. Table 3).

The Tb.N ratio indicates that *Homo*, *Gorilla* and *Pongo* have a higher trabecular number in the proximal aspect, and *Pan* have a higher number in the distal (Fig. 5D). The differences between the proximal

and distal VOI is significant for all taxa. While the Tb.N ratio differs significantly among the study sample (p=<0.001) only *Pan* shows significant pairwise results with all other taxa (p=<0.001 for all three significant tests, Sup. Table 4 and 5).

Trabecular separation

Tb.Sp differs significantly in the distal (p=<0.001) and proximal (p=0.038, Sup. Table 3) capitate of the study sample. *Gorilla* has the most widely spaced trabeculae, while *Pan* has the most tightly packed (Sup. Table 2). Pairwise comparisons indicate that distally, *Pan* is differentiated from all other taxa (Sup. Table 3). Proximally, the only significant pairwise result is between *Pan* and *Gorilla* (Fig. 4D).

The Tb.Sp ratio shows that *Homo*, *Gorilla* and *Pongo* have greater trabecular separation in the distal capitate whereas *Pan* has greater separation in the proximal (Fig. 5D, Sup. Table 5). The difference between the separation in the distal and proximal capitate is significant for all genera (Sup. Table 4). The Tb.Sp ratio differs significantly among the study sample (p=<0.001) and the results of the pairwise comparisons mirror those of the distal segment as the only significant tests are between *Pan* and the other taxa (p=<0.001 for the three significant tests, Sup. Table 4).

[FIGURE 4 ABOUT HERE]

[FIGURE 5 ABOUT HERE]

Total relative bone volume

Total BV/TV, which incorporates both trabecular and cortical bone, differs significantly across the study sample for both the proximal and distal capitate (p=<0.001 for both tests, Sup. Table 3). *Gorilla* has the highest total BV/TV in both VOIs, followed by *Pan*, *Pongo* then *Homo* (Fig. 6A, Sup. Table 2). Pairwise comparisons reveal that distally, *Homo* has significantly lower total BV/TV than all other taxa (p=<0.001 for all tests, Sup. Table 3). Proximally, the results remain the same between *Homo* and *Gorilla*, and *Homo* and *Pan*, although in this region *Homo* is undifferentiated from *Pongo*. The only significant non-human pairwise comparison among the proximal and distal results is in the distal VOI between *Pongo* and *Gorilla* (p=0.014).

The total BV/TV ratio of the proximal and distal capitate differs significantly across the study sample (p=<0.001). Pairwise comparisons reveal that *Homo* is differentiated from all non-human apes (p=<0.001 for all significant tests, Sup. Table 4) while the non-human apes are not differentiated from one another (p=0.51 for all three tests) (Fig. 6C, Sup. Table 4). The Wilcoxon signed-rank tests indicate that the differences in the total BV/TV between the two segments is statistically significant for all genera. As outlined in the above section, trabecular BV/TV is consistently higher in the proximal

segment compared to the distal segment in all genera (Fig. 4A, Sup. Table 2). However, when total BV/TV is measured, *Pan*, *Gorilla* and *Pongo* show significantly higher values in the distal capitate (Fig. 6A, Sup Table 2 and 4). In contrast, *Homo* maintains the trabecular BV/TV pattern, with higher total BV/TV in the proximal segment.

[FIGURE 6 AROUND HERE]

In the proximal capitate, the ratio of cortical bone to trabecular bone is similar among all genera, and pairwise comparisons reveal no significant results (Sup. Table 4 and 5). In this segment, the inclusion of cortical bone increases BV/TV by 24% in *Gorilla*, 29% in *Pan*, 28% in *Homo* and 24% in *Pongo*. Conversely, in the distal capitate the ratio of cortical bone to trabecular bone is statistically differentiated among the study sample (p=<0.001). Pairwise comparisons indicate this is driven by *Homo*, as the cortical bone represents a significantly lower proportion of total BV/TV compared to all other non-human apes (Sup. Table 4). The relative portions of distal cortical and trabecular bone are similar among the non-human apes with cortical bone contributing 59% of total BV/TV in *Pan* and *Pongo* and 58% for *Gorilla*. In *Homo,* cortical bone represents 38% of distal total BV/TV.

Cortical bone thickness

Ct.Th differs significantly among the study genera in both proximal and distal capitate (p=<0.001 for both tests, Sup. Table 3). In both segments *Gorilla* has the thickest mean cortical bone, followed by *Pan*, *Pongo* and finally *Homo* (Fig. 6B, Sup. Table 2). In the distal capitate, *Homo* has significantly thinner Ct.Th than the non-human apes (p=<0.001 for all tests, Sup. Table 3), while the non-human apes are not differentiated from one another. In the proximal capitate, *Homo* has significantly thinner cortical bone than *Pan* and *Gorilla* (p=<0.001) but is undifferentiated from *Pongo* (p=0.386). Across the non-human apes, *Pongo* has significantly thinner cortical bone than *Gorilla* and *Pan* (p=0.001 for both)

All genera have thicker cortical bone in the distal VOI and the difference between the proximal and distal segments is statistically significant in all genera (p=<0.001 for all tests) (Fig. 6D, Sup. Table 4 and 5). *Pongo* has the greatest relative cortical thickening in the distal VOI with the distal cortex being 79% thicker than the proximal, followed by *Gorilla* (62% thicker), *Pan* (52% thicker) and finally *Homo* (12% thicker). Pairwise comparisons of the ratio indicate that *Homo* is differentiated from all non-human apes (p=<0.001 for all tests, Sup. Table 4). There are no significant pairwise comparisons between the non-human apes. The relative thickness of the cortex and trabeculae is visualized in Fig. 7. In non-human apes, the thickest bone is consistently seen within the distal cortex. In *Homo*, the cortex and trabeculae have a similar thickness across the entire bone.

[FIGURE 7 AROUND HERE]

Allometry

The results of the allometry tests are reported in Table 3 and a figure plotting the regressions is provided in the supplementary material (Sup. Figure 2). Trabecular and total BV/TV show a significant positive allometric relationship with capitate volume across hominoids, however there are no significant allometric trends intraspecifically. In all inter- and intraspecific tests, DA is independent of capitate volume. Tb.Th shows significant positive allometry across the hominoids as well as in *Homo* and *Pongo*. In *Gorilla*, Tb.Th scales with isometry and in *Pan* it is uncorrelated. Across hominoids, Tb.N scales with negative allometry. Intraspecifically, only *Gorilla* has a significant relationship with Tb.N, scaling with negative allometry. Tb.Sp scales with positive allometry across hominoids. Intraspecifically only *Gorilla* has a significant relationship with Tb.Sp, scaling with positive allometry. Ct.Th scales with positive allometry across the hominoids, as well as in *Homo*, *Gorilla* and *Pongo*.

[TABLE 3 HERE]

Discussion

This study quantified the internal bone structure of the hominoid capitate using a whole-bone methodology to examine 1) whether relative and absolute differences in trabecular and cortical parameters across hominoid taxa could be correlated to inferred habitual behavior and 2) how the parameters differed inter- and intra-specifically across the proximal and distal portion of the capitate.

Allometry in the capitate

Interspecifically, the predictions for Tb.N and DA were supported while all others were rejected. The two parameters most strongly correlated with size were Tb.Th and Tb.N. This was particularly true for *Gorilla*, which had relatively strong positive scaling for Tb.Th, Tb.N and Tb.Sp, with r-squared values between 0.60-0.69. This suggests these parameters may be linked to sexual dimorphism, which is extreme in *Gorilla* (Smith & Jungers, 1997). Indeed, the largest Tb.Th and Tb.Sp, and smallest Tb.N values among the Gorillas were from males. *Pan* was the only genus that did not report at least one significant intraspecific allometric test. This indicates that capitate size differences (as a proxy for body mass differences) between *Pan troglodytes* and *Pan paniscus* have not influenced results.

The positive relationship found in BV/TV does not corroborate results of either previous study on allometry in the primate capitate (Schilling et al. 2014; Ragni, 2020) or the talus (Tsegai et al. 2017). Differences in results between this study and others may be driven by the variation in the

methodologies for calculating size or body mass. While this study used the cube root of the capitate, other studies have used the geometric mean (Schilling et al. 2014; Tsegai et al. 2017), body mass (Cotter et al. 2009; Barak et al. 2013), or linear dimensions of the bone (Ryan & Shaw, 2013). Furthermore, this study used a whole-bone mean of trabecular parameters whereas other studies have used a VOI sampling sphere (Cotter et al. 2009; Ryan & Shaw, 2013; Schilling et al. 2014; Ragni, 2020). Results are likely also affected by the species constituting the study sample or the bone used for analysis (Ruff, 1987; Doube et al. 2009; Ryan & Shaw, 2013; Tsegai et al. 2017). Nevertheless, as BV/TV is widely reported as being independent of body mass/size, results here may indicate carpals are more likely than other skeletal elements to increase BV/TV in response to size, across hominoids. However, given the similarity in capitate size between *Homo*, *Pan* and *Pongo*, the positive relationship found here is likely driven by the larger size of *Gorilla*, rather than reflecting a hominoid trend.

Ct.Th also scaled positively with size across hominoids and within *Homo*, *Gorilla* and *Pongo*. Notably, the r-squared value for *Pongo* and *Gorilla* were high relative to other significant tests with 0.42 and 0.40 reported, respectively. These results may reflect sexually dimorphism in *Gorilla*, as the highest Ct.Th values were all found in males, however the results were not so clear-cut in *Pongo*, with females represented within some of the highest values. The four highest Ct.Th values in *Homo* were male, however, there was a large number of specimens with unknown sex. These results, particularly the relative strength of the r-squared value, deviate from other Ct.Th studies that, for example, reported isometry in the lumbar vertebrae (Fajardo et al. 2013), positive allometry with confidence intervals incorporating isometry in the femoral neck (Demes & Walker, 2000) or negative allometry in the radius and humerus (Doube et al. 2009).

BV/TV and Ct.Th are a primary component of bone strength and are thus critical to inferring function and functional adaptation from form (Maquer et al. 2015). The positive allometric relationship of BV/TV and Ct.Th to size found in this study potentially limits the interpretive value of these measures. However, in both measurements the coefficient of determination was small at 0.13 and 0.27, respectively. Although the average *Gorilla* capitate volume is only 3000 cubic millimeters larger than the pooled average of the other taxa, the significant results may be strongly driven by this size difference. While the significant allometric relationships of Tb.Th, Tb.N and Tb.Sp are notable, these measures are highly correlated with BV/TV and thus each is less important as a single measure than that of BV/TV for understanding bone strength and drawing behavioral inferences. Allometry is undoubtedly complex and not yet fully understood by bone biologists. The generally low r-squared values found here indicate that size did not exert a strong influence on bone parameters in our sample, but these somewhat unexpected results indicate allometry cannot be overlooked in multispecies comparisons.

Can internal bone architecture differentiate locomotor modes of hominoids?

Predictions for BV/TV were broadly supported. In trabecular and total BV/TV, knuckle-walking African apes had the highest values, *Homo* had the lowest and *Pongo* generally fell out as intermediate between the two. These intermediate values in *Pongo* were not consistently differentiated from the other taxa. For example, although *Pongo* trabecular and total BV/TV in the distal capitate was significantly greater than that of *Homo*, it was not statistically different in the proximal capitate. This pattern was not predicted given the presumed higher forces acting on the *Pongo* capitate during locomotion compared with that of *Homo* manipulation. However, previous research has found similar results with BV/TV in *Pongo* being statistically undifferentiated from *Homo* within the capitate (Schilling et al. 2014) and other skeletal elements, including the talus (Desilva & Devlin, 2012; Tsegai et al. 2013), humerus (Kivell et al. 2018) and femur (Georgiou et al. 2019).

DA in the capitate was predicted to be highest in *Gorilla* and *Pan*, intermediate in *Homo* and lowest in *Pongo*, and results did not support this prediction. DA in the distal capitate was not significantly different between the genera, suggesting that the numerous, relatively immobile articulations within this region result in a similar DA value, irrespective of hand use. *Homo* and *Pongo* had higher DA in the proximal capitate compared to the distal segment, which statistically separated them from the knuckle-walking taxa. High DA is correlated with strength along predictable loading trajectories within joints (Cotter et al. 2009; Hart et al. 2017; Hammond et al. 2018.) In *Homo,* DA in the proximal capitate may be explained by load predictability as the DTM constitutes the path of motion in a large proportion of daily activities (Schuind et al. 1994; Crisco et al. 2005; Brigstocke et al. 2014; Moritomo et al. 2014; Kaufman-Cohen et al. 2019). However, the relatively high DA in the *Pongo* proximal capitate was unexpected as it was assumed that the highly mobile joint and presumed variability in wrist postures adopted during arboreal locomotion would result in diverse loading of the proximal capitate and low DA. High DA is potentially linked to methodological limitations in quantifying directionality due to high Tb.Th or low Tb.N encapsulated by the sampling sphere (Dunmore et al. 2019). However, in this study, *Pongo* Tb.N and Tb.Th were intermediate between *Gorilla* and *Pan*, and thus this result is unlikely a consequence of methodological limitations. Although some trabecular functional adaptation studies have found low DA values for *Pongo* as predicted (Tsegai et al. 2013; Matarazzo, 2015; Kivell et al. 2018; Georgiou et al. 2018) others have also found higher than expected values (Dunmore et al. 2019; Georgiou et al. 2019). Although arboreal locomotion is associated with mobile joints capable of receiving load from multiple directions, our knowledge of *Pongo* hand and wrist kinematics and kinetics is limited (but see Orr, 2010, 2017, 2018). The few studies of captive apes have provided invaluable data on the kinematics of vertical climbing (Isler, 2005; Isler & Thorpe, 2004)

and quadrupedal walking (Finestone et al. 2018; Watson et al. 2009), but these behaviors constitute a small proportion of the *Pongo* locomotor repertoire (Cant, 1987; Thorpe & Crompton, 2006). Additionally, we currently lack manual pressure research on *Pongo* similar to that by Wunderlich and Jungers (2009) or Matarazzo (2013) on African apes. This research landscape may be limiting our ability to predict and interpret functional adaptation in the wrist and hand of wild *Pongo.* Nevertheless, the DA results here indicate that *Pongo* may have less variation in its wrist or hand postures than predicted with bone aligning to high loads from a low number of habitual postures.

The significantly more isotropic structure in the proximal capitate of knuckle-walkers was also unexpected as the low range of extension during knuckle-walking was assumed to result in high DA. Nevertheless, the DA results are contained within the range of values reported by Ragni (2020) for the *Gorilla* and *Pan* proximal capitate. Dunmore et al. (2019) similarly found the sub-articular trabecular structure of the metacarpophalangeal joint in African apes to be more isotropic than predicted. While African apes are categorized as terrestrial knuckle-walkers, they also utilize arboreal substrates variably across their lifetimes to nest and exploit high quality food resources (Remis, 1995; Thorpe & Crompton, 2006; Neufuss et al. 2017). The isotropic structure may be a reflection of diverse hand postures and loading patterns from their mixed terrestrial and arboreal locomotor repertoire. It is possible these isotropic results are an artefact of high BV/TV lowering overall DA measurements and indeed in this study the lower proximal BV/TV values of *Homo* and *Pongo* are associated with higher DA. However, the similar DA values in the distal capitate, despite diverse BV/TV values, suggests our method is able to capture variation in DA across a range of BV/TV values.

This study also investigated potential differences in ratios of bone parameters across the proximal and distal capitate, testing the null hypothesis that these ratios would be similar across hominoids. This hypothesis was generally not supported as only two ratios were statistically similar across all genera: distal trabecular BV/TV relative to proximal trabecular BV/TV and proximal total BV/TV relative to proximal trabecular BV/TV. Thus, although proximal Ct.Th in *Homo* and *Pongo* was significantly thinner than that of *Pan* and *Gorilla*, the relative proportion of cortex to trabeculae is similar across all taxa. Similarly, although eight of the 12 pairwise comparisons indicated statistically different trabecular BV/TV across the taxa (Fig. 4A), the way trabecular volume differs between the two segments is consistent across hominoids. Although it was not predicted that ratio calculations would differentiate locomotor groups, three ratios distinguished *Homo* from the suspensory and knuckle-walking taxa: 1) distal total BV/TV relative to proximal total BV/TV, 2) distal total BV/TV relative to distal trabecular BV/TV, and 3) distal Ct.Th relative to proximal Ct.Th. Together, these ratios indicate that relatively low Ct.Th in the *Homo* distal capitate is distinctive compared with the thicker cortex in non-human apes. As Ct.Th is correlated to bone strength (Augat & Schorlemmer, 2006), the distal

capitate in non-human apes is likely to be better able to resist fracture or failure and withstand high mechanical loads imposed upon the region.

This distinctive cortical morphology in non-human apes may reflect arboreal behaviors. All non-human apes engage in suspensory locomotion and climb vertical supports (Remis, 1995; Thorpe & Crompton, 2006; Neufuss et al. 2017), and in both behaviors the forelimbs are loaded in tension (Swartz et al. 1989; Hunt et al. 1996; Hanna et al. 2017). The distal capitate has numerous ligament attachments that induce tensional strain onto the capitate (Kijima & Viegas, 2009; Regal et al. 2020). Bones loaded in tension have a lower failure point than those loaded in compression (Caler & Carter, 1989; Pattin et al. 1996) and therefore greater BV/TV or Ct.Th would be required to prevent failure at ligament attachment sites (Doube et al. 2009).

When comparing differences in Tb.Th, Tb.N and Tb.Sp across our study sample, results were similar to those of previous studies of different skeletal elements; *Pan* had high Tb.N and low Tb.Th and Tb.Sp, *Gorilla* showed the inverse, while *Homo* and *Pongo* were intermediate for all of these measures (Scherf et al. 2013; Schilling et al. 2014; Ryan & Shaw, 2015; Georgiou et al. 2018; Kivell et al. 2018; Georgiou et al. 2019; Komza & Skinner, 2019; Ragni, 2020). The consistent pattern within these parameters may represent systemic, rather than strongly functionally adaptive features of bone. DA and BV/TV have been shown to account for up to 98% of bone's elastic modulus (Maquer et al. 2015) and as Tb.Th, Tb.N and Tb.Sp interact via various combinations to produce BV/TV, individual measures of Tb.Th, Tb.N and Tb.Sp may be less useful for differentiating locomotor or postural modes.

Do the proximal and distal segments reflect divergent strain patterns across the capitate?

Given differences in the articulations and mobility between the proximal and distal capitate, we hypothesized that each portion would show statistically different bone structure. This hypothesis was broadly supported but there was only partial support for the specific predictions. With only two exceptions (*Pongo* distal BV/TV relative to proximal BV/TV, and *Homo* distal Tb.Th relative to proximal Tb.Th), bone parameters differed significantly between the proximal and distal regions. This suggests that the internal bone is subjected to different forces and functional adaptation responses across the capitate. Ct.Th, DA and BV/TV were predicted to be higher in the distal relative to the proximal capitate due to the immobility in the distal carpal row and numerous ligament attachments. Ct.Th results in all genera supported this prediction while the DA prediction was only supported for *Gorilla* and *Pan*. All genera had significantly higher trabecular BV/TV in the proximal capitate, however, due to the great cortical thickening in non-human apes, total BV/TV was higher in the distal capitate of *Gorilla*, *Pan* and

Pongo. In contrast, despite a 12% increase in distal Ct.Th, *Homo* maintained significantly higher total BV/TV in the proximal capitate. These differences in bone architecture were only revealed by holistically analyzing biomechanically meaningful sub-regions of the capitate, while whole-bone measures or the exclusion of cortical bone, likely would have obscured or failed to pick up these trends.

While we argue that the results of this study indicate that force transfer differs across the proximal and distal capitate, additional analyses comparing different portions of the capitate are warranted to further test this conclusion. While this study averaged parameters across entire segments, bone volume distribution methods such as those used in Tsegai et al. (2013) and Tsegai et al. (2017) would allow more nuanced analysis between the regions under compression versus tension. Further, these methods would allow a deeper exploration of the biomechanical consequences of waisted versus non-waisted capitates and whether this aspect of morphology impacts the functional independence of the proximal and distal regions.

The relationship between trabecular and cortical bone in the capitate

This study reveals the importance of considering both cortical and trabecular bone in functional adaptation research, rather than investigating each tissue separately. As exhibited in Figures 6 and 7, and discussed above, the cortical bone of the non-human ape capitate varied substantially from that of humans. Thus, the null hypothesis that the ratios of cortical to trabecular bone would be similar across the hominoids was not supported. However, there was one notable exception, namely that all the study taxa had similar cortical to trabeculae ratios in the proximal capitate.

The differences between the proximal and distal Ct.Th across the locomotor groups provide support for the hypothesis that thick distal cortex in the non-human apes is a result of functional adaptation. However, research indicates modern *Homo sapiens* have systemically low BV/TV and Ct.Th, which has been hypothesized to correlate with increased sedentism after the transition to an agricultural lifestyle (Ruff, 2005; Chirchir et al. 2015; Ryan & Shaw, 2015; Saers et al. 2016; Tsegai et al. 2018). Thus it would be valuable to assess the distal Ct.Th of pre-Holocene *Homo sapiens* to further interrogate whether thick distal Ct.Th can be correlated simply with higher loading more generally, or, as hypothesized here, is related to forelimb involvement in arboreal behavior among the non-human apes. Further, there are important limitations to our interpretation of cortical bone functional adaptation in short bones. Although cortical bone does model its structure during adulthood in response to load, the genetic blueprint and the process of modelling during ontogeny greatly determines cortical bone geometry (Martin et al. 1998; Lovejoy et al. 2003). Investigation on the changes to cortical bone geometry as a result of functional adaptation have predominantly focused

on changes at the mid-shaft of long bones (for examples and summary see Ruff et al. (2006) and references therein). In short bones there is unlikely to be the same capacity for the cortical bone to substantially change its geometry with modelling processes because, unlike the diaphysis of a long bone, there is not substantial room to expand (Martin et al. 1998). During adulthood, cortical bone commonly adapts its mechanical properties via changes to porosity, apparent mineral density or cellular anisotropy (Martin et al. 1998; Currey, 2002), changes that require different methodologies to assess (e.g histology). Finally, when segmenting different bone tissues, it can be challenging to identify the boundary between cortex and trabeculae, particularly when the cortex is porous or trabeculae are especially thick. This was a particular challenge in some of the non-human ape capitate specimens (see Sup. Figure 1) and will likely be a limitation for many short bones, depending on the question being addressed.

Conclusion

The capitate of knuckle-walking African apes and suspensory *Pongo* was differentiated from bipedal *Homo,* primarily, by thick distal cortical bone. African apes were further differentiated from *Pongo* and *Homo* by relatively isotropic trabeculae in the proximal capitate, which was not expected given the (presumably) more stereotypical loading of the wrist during knuckle-walking. However this higher than expected DA of the capitate head in *Homo* may indicate preferential alignment of trabeculae along the DTM. Although the wrist is often conceptualized as broadly being under compression or tension, the differentiated bone architecture in the proximal and distal regions of the capitate suggests that the loading environment can differ significantly even within the small bones of the carpus and highly localized functional adaptation responses may be taking place. Further, differences in cortical bone were critical for differentiating *Homo* from non-human apes. While an unexpected positive relationship was found between bone volume and capitate size, the low coefficient of determination indicated size did not strongly influence group differences in bone microstructure. Given the complex biomechanical environment, and our limited understanding of inter-carpal motion, (particularly in non-human apes) functional adaptation research of the carpals should take a holistic approach, including incorporated analysis of cortical bone.

Acknowledgements: This research was supported by a 50th Anniversary Research Scholarship, University of Kent (EEB), FP7 European Research Council Starting Grant #336301, European Union's Horizon 2020 research and innovation programme Grant #819960 and the Max Planck Society (MMS, TLK). For providing access to the specimens we would like to acknowledge: G. Haszprunar, Bavarian State Collection of Zoology; Frieder Mayer and Christiane Funk, Berlin Museum für Naturkunde; T.

Biers and M. Mirazon Lahr, the Duckworth Collection, University of Cambridge; V. Volpato and K. Krohmann, Frankfurt Senckenberg Museum; B. Groβkopf, Georg-August-University Goettingen, Anthropology Collection; C. Boesch, Max Planck Institute for Evolutionary Anthropology; I. Livne, Powell-Cotton Museum; E. Gilissen and W. Wendelen, Royal Museum for Central Africa; J. Moggi-Cecchi and S. Bortoluzzi, University of Florence; M. Teschler-Nicola and R. Muehl, Vienna Natural History Museum. For microCT scanning, we thank R. Freeney, P. Schoenfeld, A. Silvester, K. Smithson, N. Stephens, H. Temming, Z. Tsegai, and A. Winzer. The authors declare no conflicts of interest. We also thank the two anonymous reviewers for their thoughtful commentary on early versions of this manuscript. The authors declare no conflicts of interest.

Author contributions

EEB conceived and designed the experiments, acquired data, performed the experiments, analyzed the data, prepared figures and tables, authored first draft and reviewed drafts of the paper, approved the final draft.

TLK and MMS conceived and designed the experiments, contributed data, provided analysis tools, authored and provided critical review of manuscript drafts, approved the final manuscript.

References

Augat P, Schorlemmer S (2006) The role of cortical bone and its microstructure in bone strength. *Age and Ageing,* **35,** ii27-ii31.

Barak MM, Lieberman DE, Hublin J-J (2011) A Wolff in sheep's clothing: trabecular bone adaptation in response to changes in joint loading orientation. *Bone,* **49,** 1141-1151.

Barak MM, Lieberman DE, Hublin J-J (2013) Of mice, rats and men: trabecular bone architecture in mammals scales to body mass with negative allometry. *Journal of structural biology,* **183,** 123-131.

Barak MM, Weiner S, Shahar R (2010) The contribution of trabecular bone to the stiffness and strength of rat lumbar vertebrae. *Spine,* **35,** E1153-9.

Begun DR (2004) Knuckle-walking and the origin of human bipedalism. In *From Biped to Strider*), pp. 9-33. Springer.

Brainerd EL, Baier DB, Gatesy SM, et al. (2010) X-ray reconstruction of moving morphology (XROMM): precision, accuracy and applications in comparative biomechanics research. *Journal of Experimental Zoology Part A: Ecological Genetics and Physiology,* **313,** 262-279.

761 Brigstocke GHO, Hearnden A, Holt C, Whatling G (2014) In-vivo confirmation of the use of the dart
762 thrower's motion during activities of daily living. *Journal of Hand Surgery (European*
763 *Volume),* **39,** 373-378.
764 Caler WE, Carter DR (1989) Bone creep-fatigue damage accumulation. *Journal of Biomechanics,* **22,**
765 625-635.
766 Cant JG (1987) Positional behavior of female Bornean orangutans (Pongo pygmaeus). *American*
767 *Journal of Primatology,* **12,** 71-90.
768 Carlson KJ, Patel BA (2006) Habitual use of the primate forelimb is reflected in the material
769 properties of subchondral bone in the distal radius. *Journal of anatomy,* **208,** 659-670.
770 Chirchir H, Kivell TL, Ruff CB, et al. (2015) Recent origin of low trabecular bone density in modern
771 humans. *Proceedings of the National Academy of Sciences of the United States of America,*
772 **112,** 366-371.
773 Christen P, Ito K, van Rietbergen B (2015) A potential mechanism for allometric trabecular bone
774 scaling in terrestrial mammals. *Journal of anatomy,* **226,** 236-243.
775 Christen P, Schulte FA, Zwahlen A, et al. (2016) Voxel size dependency, reproducibility and sensitivity
776 of an in vivo bone loading estimation algorithm. *Journal of The Royal Society Interface,* **13,**
777 20150991.
778 Cooper D, Kawalilak C, Harrison K, Johnston B, Johnston J (2016) Cortical bone porosity: what is it,
779 why is it important, and how can we detect it? *Current osteoporosis reports,* **14,** 187-198.
780 Cotter MM, Simpson SW, Latimer BM, Hernandez CJ (2009) Trabecular microarchitecture of
781 hominoid thoracic vertebrae. *The Anatomical Record: Advances in Integrative Anatomy and*
782 *Evolutionary Biology: Advances in Integrative Anatomy and Evolutionary Biology,* **292,** 1098-
783 1106.
784 Crisco JJ, Coburn JC, Moore DC, Akelman E, Weiss A-PC, Wolfe SW (2005) In vivo radiocarpal
785 kinematics and the dart thrower's motion. *JBJS,* **87,** 2729-2740.
786 Crisco JJ, Heard WM, Rich RR, Paller DJ, Wolfe SW (2011) The mechanical axes of the wrist are
787 oriented obliquely to the anatomical axes. *The Journal of bone and joint surgery.American*
788 *volume,* **93,** 169-177.
789 Currey JD (2002) *Bones; Structure and Mechanics,* Princeton University Press.
790 Dainton M, Macho GA (1999) Did knuckle walking evolve twice? *Journal of human evolution,* **36,** 171-
791 194.
792 Demes B, Jungers WL, Walker C (2000) Cortical bone distribution in the femoral neck of strepsirhine
793 primates. *Journal of human evolution,* **39,** 367-379.

DeSilva JM, Devlin MJ (2012) A comparative study of the trabecular bony architecture of the talus in humans, non-human primates, and Australopithecus. *Journal of human evolution,* **63,** 536-551.

Doran DM (1993) Sex differences in adult chimpanzee positional behavior: the influence of body size on locomotion and posture. *American Journal of Physical Anthropology,* **91,** 99-115.

Doube M, Conroy AW, Christiansen P, Hutchinson JR, Shefelbine S (2009) Three-dimensional geometric analysis of felid limb bone allometry. *PloS one,* **4,** e4742.

Doube M, Kłosowski MM, Arganda-Carreras I, et al. (2010) BoneJ: free and extensible bone image analysis in ImageJ. *Bone,* **47,** 1076-1079.

Doube M, Klosowski MM, Wiktorowicz-Conroy AM, Hutchinson JR, Shefelbine SJ (2011) Trabecular bone scales allometrically in mammals and birds. *Proceedings.Biological sciences,* **278,** 3067-3073.

Dunmore CJ, Bardo A, Skinner MM, Kivell TL (2020) Trabecular variation in the first metacarpal and manipulation in hominids. *American Journal of Physical Anthropology,* **171,** 219-241.

Dunmore CJ, Kivell TL, Bardo A, Skinner MM (2019) Metacarpal trabecular bone varies with distinct hand-positions used in hominid locomotion. *Journal of anatomy*.

Dunmore CJ, Wollny G, Skinner MM (2018) MIA-Clustering: a novel method for segmentation of paleontological material. *PeerJ,* **6,** e4374.

Fajardo RJ, Desilva JM, Manoharan RK, Schmitz JE, Maclatchy LM, Bouxsein ML (2013) Lumbar vertebral body bone microstructural scaling in small to medium-sized strepsirhines. *The Anatomical Record,* **296,** 210-226.

Finestone EM, Brown MH, Ross SR, Pontzer H (2018) Great ape walking kinematics: Implications for hominoid evolution. *American Journal of Physical Anthropology,* **166,** 43-55.

Fragaszy DM, Crast J (2016) Functions of the hand in primates. In *The evolution of the primate hand*), pp. 313-344. Springer.

Frost HM (1987) Bone "mass" and the "mechanostat": a proposal. *The Anatomical Record,* **219,** 1-9.

Garcia-Elias M, Smith DK, Ruby LK, et al. (1994) Normal and abnormal carpal kinematics. In *Advances in the biomechanics of the hand and wrist*), pp. 247-253. Springer.

Gatesy SM, Baier DB, Jenkins FA, Dial KP (2010) Scientific rotoscoping: a morphology-based method of 3-D motion analysis and visualization. *Journal of Experimental Zoology Part A: Ecological Genetics and Physiology,* **313,** 244-261.

Georgiou L, Dunmore CJ, Bardo A, et al. (2020) Evidence for habitual climbing in a Pleistocene hominin in South Africa. *Proceedings of the National Academy of Sciences of the United States of America,* **117,** 8416-8423.

828 Georgiou L, Kivell TL, Pahr DH, Buck LT, Skinner MM (2019) Trabecular architecture of the great ape
829 and human femoral head. *Journal of anatomy,* **234,** 679-693.
830 Georgiou L, Kivell TL, Pahr DH, Skinner MM (2018) Trabecular bone patterning in the hominoid distal
831 femur. *PeerJ,* **6,** e5156.
832 Griffin NL, D'Août K, Ryan TM, Richmond BG, Ketcham RA, Postnov A (2010) Comparative forefoot
833 trabecular bone architecture in extant hominids. *Journal of human evolution,* **59,** 202-213.
834 Gross T, Kivell TL, Skinner MM, Nguyen H, Pahr DH (2014) Holistic analysis of bone. *Palaeontologia*
835 *Electronica,* **17,** 1.
836 Guo XE (2001) Mechanical properties of cortical bone and cancellous bone tissue. *Bone mechanics*
837 *handbook,* **10,** 1-23.
838 Hammond MA, Wallace JM, Allen MR, Siegmund T (2018) Incorporating tissue anisotropy and
839 heterogeneity in finite element models of trabecular bone altered predicted local stress
840 distributions. *Biomechanics and modeling in mechanobiology,* **17,** 605-614.
841 Hanna JB, Granatosky MC, Rana P, Schmitt D (2017) The evolution of vertical climbing in primates:
842 evidence from reaction forces. *Journal of Experimental Biology,* **220,** 3039-3052.
843 Hart NH, Nimphius S, Rantalainen T, Ireland A, Siafarikas A, Newton R (2017) Mechanical basis of
844 bone strength: influence of bone material, bone structure and muscle action. *Journal of*
845 *musculoskeletal & neuronal interactions,* **17,** 114.
846 Hildebrand T, Rüegsegger P (1997) A new method for the model-independent assessment of
847 thickness in three-dimensional images. *Journal of microscopy,* **185,** 67-75.
848 Hunt KD (1992) Positional behavior of Pan troglodytes in the Mahale mountains and Gombe stream
849 national parks, Tanzania. *American Journal of Physical Anthropology,* **87,** 83-105.
850 Inouye SE (1994) Ontogeny of knuckle-walking hand postures in African apes. *Journal of human*
851 *evolution,* **26,** 459-485.
852 Isaksson H, Töyräs J, Hakulinen M, et al. (2011) Structural parameters of normal and osteoporotic
853 human trabecular bone are affected differently by microCT image resolution. *Osteoporosis*
854 *international,* **22,** 167-177.
855 Isler K (2005) 3D-kinematics of vertical climbing in hominoids. *American Journal of Physical*
856 *Anthropology: The Official Publication of the American Association of Physical*
857 *Anthropologists,* **126,** 66-81.
858 Isler K, Thorpe SK (2003) Gait parameters in vertical climbing of captive, rehabilitant and wild
859 Sumatran orang-utans (Pongo pygmaeus abelii). *Journal of Experimental Biology,* **206,** 4081-
860 4096.

Jenkins FA, Fleagle JG (1975) Knuckle-walking and the functional anatomy of the wrists in living apes. *Primate functional morphology and evolution*, 213-227.

Jouffroy FK, Medina MF (2002) Radio-ulnar deviation of the primate carpus: an X-ray study. *Zeitschrift für Morphologie und Anthropologie*, 275-289.

Kalkwarf HJ, Specker BL (1995) Bone mineral loss during lactation and recovery after weaning. *Obstetrics & Gynecology,* **86,** 26-32.

Kaufman-Cohen Y, Portnoy S, Levanon Y, Friedman J (2019) Does Object Height Affect the Dart Throwing Motion Angle during Seated Activities of Daily Living? *Journal of motor behavior*, 1-10.

Kijima Y, Viegas SF (2009) Wrist anatomy and biomechanics. *The Journal of hand surgery,* **34,** 1555-1563.

Kivell TL (2016) The primate wrist. In *The Evolution of the Primate Hand*), pp. 17-54. Springer.

Kivell TL (2016) A review of trabecular bone functional adaptation: what have we learned from trabecular analyses in extant hominoids and what can we apply to fossils? *Journal of anatomy,* **228,** 569-594.

Kivell TL, Davenport R, Hublin JJ, Thackeray JF, Skinner MM (2018) Trabecular architecture and joint loading of the proximal humerus in extant hominoids, Ateles, and Australopithecus africanus. *American Journal of Physical Anthropology,* **167,** 348-365.

Kivell TL, Schmitt D (2009) Independent evolution of knuckle-walking in African apes shows that humans did not evolve from a knuckle-walking ancestor. *Proceedings of the National Academy of Sciences of the United States of America,* **106,** 14241-14246.

Komza K, Skinner MM (2019) First metatarsal trabecular bone structure in extant hominoids and Swartkrans hominins. *Journal of human evolution,* **131,** 1-21.

Lewis OJ (1977) Joint remodelling and the evolution of the human hand. *Journal of anatomy,* **123,** 157-201.

Lewis OJ (1989) *Functional morphology of the evolving hand and foot,* Oxford University Press, USA.

Lieberman DE (1996) How and why humans grow thin skulls: experimental evidence for systemic cortical robusticity. *American Journal of Physical Anthropology: The Official Publication of the American Association of Physical Anthropologists,* **101,** 217-236.

Lieberman DE (1997) Making behavioral and phylogenetic inferences from hominid fossils: considering the developmental influence of mechanical forces. *Annual Review of Anthropology,* **26,** 185-210.

Lovejoy CO, McCollum MA, Reno PL, Rosenman BA (2003) Developmental biology and human evolution. *Annual Review of Anthropology,* **32,** 85-109.

Manduell KL, Morrogh-Bernard HC, Thorpe SKS (2011) Locomotor behavior of wild orangutans (Pongo pygmaeus wurmbii) in disturbed peat swamp forest, Sabangau, Central Kalimantan, Indonesia. *American Journal of Physical Anthropology,* **145,** 348-359.

Maquer G, Musy SN, Wandel J, Gross T, Zysset PK (2015) Bone volume fraction and fabric anisotropy are better determinants of trabecular bone stiffness than other morphological variables. *Journal of bone and mineral research,* **30,** 1000-1008.

Martin RB, Burr DB, Sharkey NA (1998) *Skeletal tissue mechanics,* Springer.

Marzke MW (1983) Joint functions and grips of the Australopithecus afarensis hand, with special reference to the region of the capitate. *Journal of human evolution,* **12,** 197-211.

Marzke MW (1997) Precision grips, hand morphology, and tools. *American Journal of Physical Anthropology,* **102,** 91-110.

Marzke MW, Marzke RF (1987) The third metacarpal styloid process in humans: origin and functions. *American Journal of Physical Anthropology,* **73,** 415-431.

Matarazzo S (2013) Manual pressure distribution patterns of knuckle-walking apes. *American Journal of Physical Anthropology,* **152,** 44-50.

Matarazzo SA (2015) Trabecular architecture of the manual elements reflects locomotor patterns in primates. *PloS one,* **10,** e0120436.

Mielke M, Wölfer J, Arnold P, van Heteren AH, Amson E, Nyakatura JA (2018) Trabecular architecture in the sciuromorph femoral head: allometry and functional adaptation. *Zoological letters,* **4,** 10.

Moojen TM, Snel JG, Ritt MJ, Venema HW, Kauer JM, Bos KE (2003) In vivo analysis of carpal kinematics and comparative review of the literature. *The Journal of hand surgery,* **28,** 81-87.

Moritomo H, Apergis EP, Herzberg G, Werner FW, Wolfe SW, Garcia-Elias M (2014) IFSSH scientific committee on anatomy and biomechanics wrist biomechanics and instability: Wrist dart-throwing motion updated. *International Federation of Societies for Surgery of the Hand***,** 23-28.

Napier JR (1956) The prehensile movements of the human hand. *The Journal of bone and joint surgery.British volume,* **38,** 902-913.

Neufuss J, Robbins MM, Baeumer J, Humle T, Kivell TL (2017) Comparison of hand use and forelimb posture during vertical climbing in mountain gorillas (Gorilla beringei beringei) and chimpanzees (Pan troglodytes). *American journal of physical anthropology,* **164,** 651-664.

Niewoehner WA, Weaver AH, Trinkaus E (1997) Neandertal capitate-metacarpal articular morphology. *American Journal of Physical Anthropology: The Official Publication of the American Association of Physical Anthropologists,* **103,** 219-233.

Orr CM (2005) Knuckle-walking anteater: A convergence test of adaptation for purported knuckle-walking features of african Hominidae. *American Journal of Physical Anthropology: The Official Publication of the American Association of Physical Anthropologists,* **128,** 639-658.

Orr CM (2010) *Adaptations to knuckle-walking and digitigrady: a three-dimensional kinematic and morphometric analysis of the anthropoid wrist,* Arizona State University.

Orr CM (2016) Functional morphology of the primate hand: Recent approaches using biomedical imaging, computer modeling, and engineering methods. In *The Evolution of the Primate Hand*), pp. 227-257. Springer.

Orr CM (2017) Locomotor hand postures, carpal kinematics during wrist extension, and associated morphology in anthropoid primates. *The Anatomical Record,* **300,** 382-401.

Orr CM (2018) Kinematics of the anthropoid os centrale and the functional consequences of scaphoid-centrale fusion in African apes and hominins. *Journal of human evolution,* **114,** 102-117.

Orr CM, Leventhal EL, Chivers SF, Marzke MW, Wolfe SW, Crisco JJ (2010) Studying Primate Carpal Kinematics in Three Dimensions Using a Computed-Tomography-Based Markerless Registration Method. *The Anatomical Record: Advances in Integrative Anatomy and Evolutionary Biology,* **293,** 692-709.

Pahr DH, Zysset PK (2009) A comparison of enhanced continuum FE with micro FE models of human vertebral bodies. *Journal of Biomechanics,* **42,** 455-462.

Pahr DH, Zysset PK (2009) From high-resolution CT data to finite element models: development of an integrated modular framework. *Computer methods in biomechanics and biomedical engineering,* **12,** 45-57.

Parsons TJ, Van Dusseldorp M, van Der Vliet M, Van De Werken K, Schaafsma G, Van Staveren WA (1997) Reduced bone mass in Dutch adolescents fed a macrobiotic diet in early life. *Journal of Bone and Mineral Research,* **12,** 1486-1494.

Paternoster L, Lorentzon M, Lehtimäki T, et al. (2013) Genetic determinants of trabecular and cortical volumetric bone mineral densities and bone microstructure. *PLoS genetics,* **9,** e1003247.

Pattin CA, Caler WE, Carter DR (1996) Cyclic mechanical property degradation during fatigue loading of cortical bone. *Journal of Biomechanics,* **29,** 69-79.

Pettersson U, Nilsson M, Sundh V, Mellström D, Lorentzon M (2010) Physical activity is the strongest predictor of calcaneal peak bone mass in young Swedish men. *Osteoporosis International,* **21,** 447-455.

963 Pontzer H, Lieberman DE, Momin E, et al. (2006) Trabecular bone in the bird knee responds with
964 high sensitivity to changes in load orientation. *The Journal of experimental biology,* **209,** 57-
965 65.
966 Ragni AJ (2020) Trabecular architecture of the capitate and third metacarpal through ontogeny in
967 chimpanzees (Pan troglodytes) and gorillas (Gorilla gorilla). *Journal of human evolution,* **138,**
968 102702.
969 Regal S, Maschke S, Li Z-M (2020) Hand and Wrist Biomechanics. In *Frontiers in Orthopaedic*
970 *Biomechanics*), pp. 89-104. Springer.
971 Rein TR, Harvati K (2013) Exploring third metacarpal capitate facet shape in early hominins. *The*
972 *Anatomical Record,* **296,** 240-249.
973 Remis M (1995) Effects of body size and social context on the arboreal activities of lowland gorillas in
974 the Central African Republic. *American Journal of Physical Anthropology,* **97,** 413-433.
975 Remis MJ (1998) The gorilla paradox. In *Primate locomotion*), pp. 95-106. Springer.
976 Richmond BG (2006) Functional morphology of the midcarpal joint in knuckle-walkers and terrestrial
977 quadrupeds. In *Human origins and environmental backgrounds*), pp. 105-122. Springer.
978 Richmond BG, Begun DR, Strait DS (2001) Origin of human bipedalism: the knuckle-walking
979 hypothesis revisited. *American Journal of Physical Anthropology: The Official Publication of*
980 *the American Association of Physical Anthropologists,* **116,** 70-105.
981 Riley G, Trinkaus E (1989) Neandertal capitate-metacarpal 2 articular morphology and Neandertal
982 manipulative behavior. In *American Journal of Physical Anthropology*), pp. 290-290. WILEY-
983 LISS DIV JOHN WILEY & SONS INC 605 THIRD AVE, NEW YORK, NY 10158-0012.
984 Ruff C, Holt B, Trinkaus E (2006) Who's afraid of the big bad Wolff?:“Wolff's law” and bone
985 functional adaptation. *American Journal of Physical Anthropology: The Official Publication of*
986 *the American Association of Physical Anthropologists,* **129,** 484-498.
987 Ruff CB (1984) Allometry between length and cross-sectional dimensions of the femur and tibia in
988 Homo sapiens sapiens. *American Journal of Physical Anthropology,* **65,** 347-358.
989 Ruff CB, Runestad JA (1992) Primate limb bone structural adaptations. *Annual Review of*
990 *Anthropology,* **21,** 407-433.
991 Runestad JA (1997) Postcranial adaptations for climbing in Loridae (Primates). *Journal of Zoology,*
992 **242,** 261-290.
993 Ryan TM, Shaw CN (2013) Trabecular bone microstructure scales allometrically in the primate
994 humerus and femur. *Proceedings of the Royal Society B: Biological Sciences,* **280,** 20130172.

995 Ryan TM, Shaw CN (2015) Gracility of the modern Homo sapiens skeleton is the result of decreased
996 biomechanical loading. *Proceedings of the National Academy of Sciences of the United States*
997 *of America,* **112,** 372-377.
998 Saers JPP, Cazorla-Bak Y, Shaw CN, Stock JT, Ryan TM (2016) Trabecular bone structural variation
999 throughout the human lower limb. *Journal of human evolution,* **97,** 97-108.
1000 Sarmiento EE (1988) Anatomy of the hominoid wrist joint: its evolutionary and functional
1001 implications. *International Journal of Primatology,* **9,** 281-345.
1002 Scherf H, Harvati K, Hublin JJ (2013) A comparison of proximal humeral cancellous bone of great
1003 apes and humans. *Journal of human evolution,* **65,** 29-38.
1004 Schilling AM, Tofanelli S, Hublin JJ, Kivell TL (2014) Trabecular bone structure in the primate wrist.
1005 *Journal of Morphology,* **275,** 572-585.
1006 Schuind F, An KN, Cooney Iii WP, Garcia-Elias M (2013) *Advances in the Biomechanics of the Hand*
1007 *and Wrist,* Springer Science & Business Media.
1008 Schuind F, Cooney WP, Linscheid RL, An KN, Chao EYS (1995) Force and pressure transmission
1009 through the normal wrist. A theoretical two-dimensional study in the posteroanterior plane.
1010 *Journal of Biomechanics,* **28,** 587-601.
1011 Skinner MM, Stephens NB, Tsegai ZJ, et al. (2015) Human evolution. Human-like hand use in
1012 Australopithecus africanus. *Science (New York, N.Y.),* **347,** 395-399.
1013 Smith RJ, Jungers WL (1997) Body mass in comparative primatology. *Journal of Human evolution,* **32,**
1014 523-559.
1015 Stephens NB, Kivell TL, Gross T, et al. (2016) Trabecular architecture in the thumb of Pan and Homo:
1016 implications for investigating hand use, loading, and hand preference in the fossil record.
1017 *American Journal of Physical Anthropology,* **161,** 603-619.
1018 Stephens NB, Kivell TL, Pahr DH, Hublin J-J, Skinner MM (2018) Trabecular bone patterning across
1019 the human hand. *Journal of human evolution,* **123,** 1-23.
1020 Su A, Carlson KJ (2017) Comparative analysis of trabecular bone structure and orientation in South
1021 African hominin tali. *Journal of human evolution,* **106,** 1-18.
1022 Swartz SM, Bertram JEA, Biewener AA (1989) Telemetered in vivo strain analysis of locomotor
1023 mechanics of brachiating gibbons. *Nature,* **342,** 270.
1024 Thompson NE (2020) The biomechanics of knuckle-walking: 3-D kinematics of the chimpanzee and
1025 macaque wrist, hand and fingers. *Journal of Experimental Biology,* **223**.
1026 Thompson NE, Ostrofsky KR, McFarlin SC, Robbins MM, Stoinski TS, Almécija S (2018) Unexpected
1027 terrestrial hand posture diversity in wild mountain gorillas. *American journal of physical*
1028 *anthropology,* **166,** 84-94.

Thorpe SKS, Crompton RH (2006) Orangutan positional behavior and the nature of arboreal locomotion in Hominoidea. *American Journal of Physical Anthropology: The Official Publication of the American Association of Physical Anthropologists,* **131,** 384-401.

Thorpe SKS, Crompton RH (2009) Orangutan positional behavior: interspecific variation and ecological correlates. *Orangutans: Geographic variation in behavioral ecology and conservation***,** 33-47.

Tocheri MW, Orr CM, Jacofsky MC, Marzke MW (2008) The evolutionary history of the hominin hand since the last common ancestor of Pan and Homo. *Journal of anatomy,* **212,** 544-562.

Tocheri MW, Orr CM, Larson SG, et al. (2007) The primitive wrist of Homo floresiensis and its implications for hominin evolution. *Science (New York, N.Y.),* **317,** 1743-1745.

Tsegai ZJ, Kivell TL, Gross T, et al. (2013) Trabecular bone structure correlates with hand posture and use in hominoids. *PLoS One,* **8,** e78781.

Tsegai ZJ, Skinner MM, Gee AH, et al. (2017) Trabecular and cortical bone structure of the talus and distal tibia in Pan and Homo. *American Journal of Physical Anthropology,* **163,** 784-805.

Tsegai ZJ, Skinner MM, Pahr DH, Hublin JJ, Kivell TL (2018) Systemic patterns of trabecular bone across the human and chimpanzee skeleton. *Journal of anatomy,* **232,** 641-656.

Tuttle RH (1969) Quantitative and functional studies on the hands of the Anthropoidea. I. The Hominoidea. *Journal of Morphology,* **128,** 309-363.

van Lawick-Goodall J (1968) The behaviour of free-living chimpanzees in the Gombe Stream Reserve. *Animal behaviour monographs,* **1,** 161-IN12.

Wallace IJ, Pagnotti GM, Rubin-Sigler J, et al. (2015) Focal enhancement of the skeleton to exercise correlates to mesenchymal stem cell responsivity rather than peak external forces. *Journal of Experimental Biology*.

Ward CV (2002) Interpreting the posture and locomotion of Australopithecus afarensis: where do we stand? *American Journal of Physical Anthropology,* **119,** 185-215.

Ward CV, Tocheri MW, Plavcan JM, Brown FH, Manthi FK (2014) Early Pleistocene third metacarpal from Kenya and the evolution of modern human-like hand morphology. *Proceedings of the National Academy of Sciences of the United States of America,* **111,** 121-124.

Watson J, Payne R, Chamberlain A, Jones R, Sellers W (2011) The influence of load carrying on gait parameters in humans and apes: implications for the evolution of human bipedalism. In *Primate Locomotion*), pp. 109-134. Springer.

Whitehouse WJ (1974) The quantitative morphology of anisotropic trabecular bone. *Journal of microscopy,* **101,** 153-168.

Wolfe SW, Crisco JJ, Orr CM, Marzke MW (2006) The dart-throwing motion of the wrist: is it unique to humans? *The Journal of hand surgery,* **31,** 1429-1437.

Wunderlich RE, Jungers WL (2009) Manual digital pressures during knuckle-walking in chimpanzees (Pan troglodytes). *American Journal of Physical Anthropology: The Official Publication of the American Association of Physical Anthropologists,* **139,** 394-403.

Yao J, Lian Z, Yang B, Fan Y (2020) Biomechanics of Ligaments. In *Frontiers in Orthopaedic Biomechanics*), pp. 75-87. Springer.

Yeni YN, Zinno MJ, Yerramshetty JS, Zauel R, Fyhrie DP (2011) Variability of trabecular microstructure is age-, gender-, race-and anatomic site-dependent and affects stiffness and stress distribution properties of human vertebral cancellous bone. *Bone,* **49,** 886-894.

Zeininger A, Richmond BG, Hartman G (2011) Metacarpal head biomechanics: A comparative backscattered electron image analysis of trabecular bone mineral density in Pan troglodytes, Pongo pygmaeus, and Homo sapiens. *Journal of human evolution,* **60,** 703-710.

Supplementary Material

Cortical and trabecular bone structure of the hominoid capitate

Emma E. Bird, Tracy L. Kivell, and Matthew M. Skinner

Supplementary Table 1. Downloadable excel file recording specimen information and individual parameter values. Values are recorded for the whole bone as well as the proximal and distal segments. The specimen column records the curatorial institutions as abbreviations; DCW = The Duckworth Collection, University of Cambridge; INDEN = Georg-August-University Goettingen, Anthropology Collection; MPI_TC = Max Planck Institute for Evolutionary Anthropology Primatology, Tai Collection; MRAC = Royal Museum for Central Africa Tervuren; NGB = University of Kent; NHMW = Natural History Museum Vienna; NMNH = National Museum Natural History Smithsonian; PC = Powell-Cotton Museum; SMF = Senckenberg Natural History Museum, Frankfurt; UNI_FL = University of Florence; ZMB = the Natural History Museum, Berlin; ZSM = Bavarian State Collection Zoology.

1089 Supplementary Table 2. Descriptive statistics for this study. Capitate size (mm^3) is reported for the
1090 whole bone. Trabecular and cortical bone parameters are reported for the proximal, distal and whole
1091 bone separately. ± indicates one standard deviation above and below the mean.

Capitate size (mm^3)		*Homo*	*Pan*	*Gorilla*	*Pongo*
Whole bone	Mean	2495 ± 652	2418 ± 505	5376 ± 2,403	2171 ± 568
	Range	1190 – 3606	1670 – 3634	2452 – 10200	1452 – 3182
Trabecular BV/TV (%)		*Homo*	*Pan*	*Gorilla*	*Pongo*
Proximal	Mean	0.29±0.07	0.38±0.04	0.43±0.06	0.36±0.10
	Range	0.20-0.42	0.30-0.46	0.30-0.54	0.17-0.52
Distal	Mean	0.26±0.06	0.34±0.04	0.39±0.05	0.33±0.06
	Range	0.14-0.35	0.29-0.43	0.28-0.48	0.21-0.43
Whole	Mean	0.27±0.06	0.36±0.04	0.41±0.05	0.34±0.07
	Range	0.16-0.35	0.30-0.44	0.29-0.50	0.20-0.47
DA (0-1)		*Homo*	*Pan*	*Gorilla*	*Pongo*
Proximal	Mean	0.30±0.04	0.24±0.03	0.24±0.03	0.30±0.04
	Range	0.21-0.39	0.17-0.29	0.19-0.31	0.25-0.39
Distal	Mean	0.27±0.03	0.26±0.02	0.28±0.02	0.27±0.02
	Range	0.22-0.36	0.22-0.31	0.23-0.34	0.24-0.32
Whole	Mean	0.28±0.03	0.25±0.02	0.26±0.02	0.28±0.02
	Range	0.23-0.36	0.20-0.29	0.23-0.33	0.24-0.32
Tb.Th (mm)		*Homo*	*Pan*	*Gorilla*	*Pongo*
Proximal	Mean	0.23±0.05	0.25±0.02	0.34±0.04	0.26±0.04
	Range	0.16-0.33	0.21-0.29	0.23-0.43	0.16-0.36
Distal	Mean	0.22±0.04	0.24±0.04	0.33±0.04	0.28±0.03
	Range	0.16-0.33	0.20-0.38	0.24-0.39	0.20-0.35
Whole	Mean	0.22±0.04	0.24±0.02	0.34±0.04	0.27±0.03
	Range	0.17-0.32	0.20-0.28	0.23-0.41	0.19-0.35
Tb.N (mm^{-1})		*Homo*	*Pan*	*Gorilla*	*Pongo*
Proximal	Mean	1.23±0.18	1.25±0.10	1.00±0.16	1.19±0.10
	Range	0.88-1.63	1.09-1.49	0.64-1.33	1.03-1.34
Distal	Mean	1.13±0.15	1.33±0.09	0.95±0.17	1.04±0.10
	Range	0.76-1.45	1.19-1.56	0.62-1.24	0.82-1.17
Whole	Mean	1.16±0.16	1.29±0.09	0.97±0.16	1.08±0.09

	Range	0.78-1.47	1.15-1.53	0.63-1.27	0.91-1.20
Tb.Sp (mm)		*Homo*	*Pan*	*Gorilla*	*Pongo*
Proximal	Mean	0.59±0.12	0.54±0.05	0.67±0.15	0.57±0.07
	Range	0.40-0.85	0.44-0.62	0.46-1.15	0.47-0.73
Distal	Mean	0.66±0.12	0.51±0.04	0.74±0.17	0.68±0.09
	Range	0.50-1.08	0.43-0.58	0.52-1.21	0.58-0.91
Whole	Mean	0.64±0.12	0.53±0.05	0.71±0.16	0.65±0.07
	Range	0.48-1.03	0.43-0.62	0.51-1.19	0.56-0.81
Total BV/TV (%)		*Homo*	*Pan*	*Gorilla*	*Pongo*
Proximal	Mean	0.37±0.07	0.50±0.06	0.54±0.07	0.45±0.10
	Range	0.26-0.50	0.38-0.62	0.41-0.67	0.24-0.61
Distal	Mean	0.35±0.07	0.55±0.07	0.62±0.07	0.53±0.08
	Range	0.23-0.49	0.44-0.68	0.48-0.74	0.34-0.66
Whole	Mean	0.36±0.06	0.53±0.06	0.60±0.06	0.51±0.08
	Range	0.25-0.46	0.43-0.65	0.47-0.71	0.32-0.66
Ct.Th (mm)		*Homo*	*Pan*	*Gorilla*	*Pongo*
Proximal	Mean	0.27±0.05	0.37±0.06	0.41±0.08	0.28±0.04
	Range	0.20-0.38	0.30-0.52	0.23-0.52	0.18-0.35
Distal	Mean	0.31±0.07	0.57±0.09	0.65±0.17	0.52±0.16
	Range	0.19-0.42	0.45-0.74	0.41-1.05	0.32-0.61
Whole	Mean	0.30±0.05	0.52±0.07	0.60±0.14	0.47±0.13
	Range	0.19-0.39	0.42-0.67	0.39-0.97	0.31-0.75

1092

Supplementary Table 3. Results of the Kruskal-Wallis and post-hoc pairwise comparison tests of the mean parameters in the proximal and distal segments. In the pairwise comparisons table, values above the diagonal represent the pairwise results for the distal capitate and those below the diagonal represent the results of the proximal. Significant results are in bold.

Kruskal-Wallis		Proximal		Distal		
Trabecular BV/TV		**<0.001**		**<0.001**		
DA		**<0.001**		0.593		
Tb.Th		**<0.001**		**<0.001**		
Tb.N		**<0.001**		**<0.001**		
Tb.Sp		**0.038**		**<0.001**		
Total BV/TV		**<0.001**		**<0.001**		
Ct.Th		**<0.001**		**<0.001**		
Pairwise Comparisons						
Trabecular BV/TV		*Homo*	*Pan*	*Gorilla*	*Pongo*	
Homo	Proximal		**0.001**	**<0.001**	**0.011**	Distal
Pan		**<0.001**		**0.044**	0.685	
Gorilla		**<0.001**	**0.047**		**0.040**	
Pongo		0.111	0.550	0.111		
DA		*Homo*	*Pan*	*Gorilla*	*Pongo*	
Homo	Proximal		1	1	1	Distal
Pan		**<0.001**		1	1	
Gorilla		**<0.001**	0.846		1	
Pongo		0.846	**<0.001**	**<0.001**		
Tb.Th		*Homo*	*Pan*	*Gorilla*	*Pongo*	
Homo	Proximal		0.278	**<0.001**	**0.004**	Distal
Pan		0.072		**<0.001**	**0.004**	
Gorilla		**<0.001**	**<0.001**		**0.007**	
Pongo		0.069	0.650	**<0.001**		
Tb.N		*Homo*	*Pan*	*Gorilla*	*Pongo*	
Homo	Proximal		**0.001**	**0.004**	0.173	Distal
Pan		1		**<0.001**	**<0.001**	
Gorilla		**0.001**	**<0.001**		0.173	
Pongo		1	1	**0.004**		

Tb.Sp		*Homo*	*Pan*	*Gorilla*	*Pongo*	
Homo	Proximal		**<0.001**	0.290	0.580	Distal
Pan		0.630		**<0.001**	**<0.001**	
Gorilla		0.450	**0.020**		0.580	
Pongo		0.980	0.980	0.180		
Total BV/TV		*Homo*	*Pan*	*Gorilla*	*Pongo*	
Homo	Proximal		**<0.001**	**<0.001**	**<0.001**	Distal
Pan		**<0.001**		0.034	0.519	
Gorilla		**<0.001**	0.202		**0.014**	
Pongo		0.112	0.220	0.089		
Ct.Th		*Homo*	*Pan*	*Gorilla*	*Pongo*	
Homo	Proximal		**<0.001**	**<0.001**	**<0.001**	Distal
Pan		**<0.001**		0.360	0.360	
Gorilla		**<0.001**	0.386		0.110	
Pongo		0.386	**0.001**	**0.001**		

1097

Supplementary Table 4. Results of the nine ratios and the associated inter- and intraspecific Wilcoxon tests. The results of the ratios are shown within the grey shaded cells on the diagonal. Results above 1 indicate the parameter is higher in the distal segment. Asterisks within these cells specify the results of the intraspecific Wilcoxon signed-rank test indicating whether the proximal and distal results are significantly different from one another; * = $p \leq 0.05$; ** = $p \leq 0.001$. Below the diagonal, the ratio values are the results of the interspecific pairwise comparisons of the ratio. Significant results are in bold. Descriptive statistics of the ratios can be found in Supplementary Table 5.

Segment (distal/proximal) differences		*Homo*	*Pan*	*Gorilla*	*Pongo*
Trabecular BV/TV	*Homo*	0.87**			
	Pan	1	0.90**		
	Gorilla	1	1	0.91**	
	Pongo	1	1	1	0.95
DA		*Homo*	*Pan*	*Gorilla*	*Pongo*
	Homo	0.91**			
	Pan	**<0.001**	1.09*		
	Gorilla	**<0.001**	0.283	1.15**	
	Pongo	0.981	**0.001**	**<0.001**	0.90*
Tb.Th		*Homo*	*Pan*	*Gorilla*	*Pongo*
	Homo	0.99			
	Pan	**0.001**	0.92*		
	Gorilla	0.184	**0.041**	0.96*	
	Pongo	**0.041**	**<0.001**	**0.005**	1.07*
Tb.N		*Homo*	*Pan*	*Gorilla*	*Pongo*
	Homo	0.92**			
	Pan	**<0.001**	1.06**		
	Gorilla	0.513	**<0.001**	0.94*	
	Pongo	0.093	**<0.001**	**0.039**	0.87**
Tb.Sp		*Homo*	*Pan*	*Gorilla*	*Pongo*
	Homo	1.12**			
	Pan	**<0.001**	0.94**		
	Gorilla	0.788	**<0.001**	1.11*	
	Pongo	0.356	**<0.001**	0.498	1.20**
Total BV/TV		*Homo*	*Pan*	*Gorilla*	*Pongo*

	Homo	0.94**			
	Pan	**<0.001**	1.11**		
	Gorilla	**<0.001**	0.51	1.15**	
	Pongo	**<0.001**	0.51	0.51	1.21*
Ct.Th		*Homo*	*Pan*	*Gorilla*	*Pongo*
	Homo	1.12**			
	Pan	**<0.001**	1.52**		
	Gorilla	**<0.001**	0.810	1.62**	
	Pongo	**<0.001**	0.380	0.400	1.79**
BV/TV (total/trabecular) differences		*Homo*	*Pan*	*Gorilla*	*Pongo*
Proximal	*Homo*	1.28			
	Pan	1	1.29		
	Gorilla	0.22	0.29	1.24	
	Pongo	0.36	0.31	1	1.24
		Homo	*Pan*	*Gorilla*	*Pongo*
Distal	*Homo*	1.38			
	Pan	**<0.001**	1.59		
	Gorilla	**<0.001**	1	1.58	
	Pongo	**<0.001**	1	1	1.59

1105

Supplementary Table 5. Descriptive statistics for the nine ratios calculated in this study. ± indicates one standard deviation above or below the mean.

Regional (distal/proximal) differences		*Homo*	*Pan*	*Gorilla*	*Pongo*
Trabecular BV/TV	Mean	0.87±0.07	0.90±0.03	0.90±0.04	0.94±0.14
	Range	0.64-1.00	0.82-0.96	0.82-1.20	0.71-1.20
DA	Mean	0.91±0.10	1.09±0.13	1.15±0.12	0.92±0.10
	Range	0.69-1.14	0.92-1.44	0.95-1.41	0.73-1.11
Tb.Th	Mean	0.99±0.06	0.92±0.04	0.96±0.04	1.07±0.06
	Range	0.83-1.19	0.82-0.98	0.90-1.04	0.93-1.20
Tb.N	Mean	0.92±0.05	1.06±0.03	0.94±0.07	0.87±0.06
	Range	0.78-1.00	1.00-1.11	0.83-1.19	0.73-0.97
Tb.Sp	Mean	1.12±0.09	0.94±0.03	1.11±0.11	1.20±0.14
	Range	0.99-1.34	0.89-1.00	0.78-1.29	1.01-1.51
Total BV/TV	Mean	0.94±0.08	1.11±0.07	1.15±0.05	1.21±0.17
	Range	0.75-1.12	0.98-1.21	1.06-1.27	0.93-1.53
Ct.Th	Mean	1.12±0.13	1.52±0.21	1.62±0.40	1.79±0.36
	Range	0.92-1.46	1.13-2.00	1.23-2.80	1.35-2.45
BV/TV (total/trabecular) differences		*Homo*	*Pan*	*Gorilla*	*Pongo*
Proximal	Mean	1.28±0.06	1.29±0.07	1.24±0.06	1.24±0.06
	Range	1.13-1.40	1.19-1.45	1.15-1.38	1.15-1.42
Distal	Mean	1.38±0.12	1.59±0.16	1.58±0.14	1.59±0.14
	Range	1.25-1.66	1.43-1.73	1.41-1.78	1.42-1.84

Supplementary figure 1. Example of excluded *Pan troglodytes* specimen, accession ID: PC_ZVII_24, Powell-Cotton Museum. A) CT-derived surface model of *Pan* capitate showing the location of four cross-sections. Cross-sections show dense and porous bone is continuous throughout the entire capitate. B) *Pan* specimen visualized after medtool data collection. The whole bone is shown transparent in pink, allowing visualization of the constricted and discontinuous trabecular bone region within. Results of the medtool analysis of this specimen are given in the table.

Supplementary figure 2. Plots of the seven RMA regressions testing for allometry. Individual data points are colored by genus and the hominoid trend is indicated by the dotted black line and grey confidence interval. The log cube root of the volume (mm^3) is seen across the x axis. A) Trabecular BV/TV; B) DA; C) Tb.Th.; D) Tb.N.; E) Tb.Sp.; E) Total BV/TV; G) Ct.Th.

Tables

Table 1. Summary of the hypotheses, predictions and statistical tests used in this study.

Hypothesis	Predictions	Statistical tests
#1	Between species	
Locomotor and behavioral differences among extant hominoids will result in significantly different trabecular and cortical architecture in their capitates	• Knuckle-walking taxa will exhibit high BV/TV and DA • *Pongo* will show intermediate BV/TV and low DA • *Homo* will exhibit low BV/TV and intermediate DA • Cortical bone will be thickest in *Gorilla* and *Pan*, followed by *Pongo*, then *Homo*.	• Kruskal-Wallis one-way ANOVA • Pairwise Wilcoxon rank-sum tests
#2	Between species	
Proximal and distal segments will show significantly differentiated internal bone architecture	• Distal to proximal ratios will be statistically undifferentiated among the study taxa	• Wilcoxon signed-rank test
	Within Species	
	• The distal aspect will have higher BV/TV and DA compared to the proximal aspect across all species • The distal cortex will be significantly thicker than the proximal across all species	• Kruskal-Wallis one-way ANOVA • Pairwise Wilcoxon rank-sum test
#3	Between species	
Allometry	• Only Tb.N will show a significant negative relationship to body size, while all other parameters will be uncorrelated	• Reduced major axis regression
	Within species	Within species
	• No parameters will exhibit significant correlations with body size	• Reduced major axis regression

1125 Table 2. Summary of study sample

Taxon	N	Side		Sex			Behavioral Group
		Right	Left	Female	Male	Unknown	
Homo sapiens	26	14	12	5	9	12	Bipedal/Manipulative
Pan paniscus	8	5	3	4	4		Knuckle-Walking
Pan troglodytes	6	3	3	3	3		Knuckle-Walking
Gorilla beringei	1		1			1	Knuckle-Walking
Gorilla gorilla	15	8	7	7	7	1	Knuckle-Walking
Pongo abelii	2	1	1	1	1		Suspensory
Pongo pygmaeus	11	6	5	5	4	2	Suspensory

1126

1127

1128 Table 3. RMA regression results of the inter- and interspecific allometry. CL- and CL+ indicate the 95%
1129 lower and upper limits for the confidence interval. Significant test are in bold.

	Variable	Isometric slope	Slope	CL-	CL+	r^2	Intercept	p-value	Allometry
Whole sample	BV/TV	0	1.800	1.440	2.250	0.133	-2.550	**0.001**	**Positive**
	DA	0	-0.759	-0.966	-0.596	0.005	0.310	0.559	Uncorrelated
	Tb.Th	1	1.480	1.240	1.770	0.460	-2.280	**<0.001**	**Positive**
	Tb.N	0	-1.140	-1.390	-0.940	0.362	1.360	**<0.001**	**Negative**
	Tb.Sp	1	1.290	1.040	1.600	0.187	-1.680	**<0.001**	**Positive**
	Total BV/TV	0	1.830	1.460	2.280	0.150	-2.420	**0.001**	**Positive**
	Ct.Th	1	2.430	1.980	2.980	0.278	-3.160	**<0.001**	**Positive**
Homo	BV/TV	0	2.600	1.760	3.840	0.095	-3.510	0.125	Uncorrelated
	DA	0	1.190	0.799	1.760	0.068	-1.880	0.198	Uncorrelated
	Tb.Th	1	1.970	1.370	2.810	0.244	-2.860	**0.010**	**Positive**
	Tb.N	0	-1.630	-2.420	-1.100	0.066	1.900	0.205	Uncorrelated
	Tb.Sp	1	1.990	1.320	2.990	0.009	-2.440	0.629	Uncorrelated
	Total BV/TV	0	2.160	1.450	3.210	0.064	-2.880	0.212	Uncorrelated
	Ct.Th	1	1.980	1.370	2.870	0.194	-2.760	**0.024**	**Positive**
Pan	BV/TV	0	-1.770	-3.140	-0.998	0.070	1.550	0.341	Uncorrelated
	DA	0	1.390	0.785	2.470	0.070	-2.160	0.344	Uncorrelated
	Tb.Th	1	-1.520	-2.710	-0.850	0.068	1.100	0.384	Uncorrelated
	Tb.N	0	1.140	0.628	2.060	<0.001	-1.170	0.976	Uncorrelated
	Tb.Sp	1	1.480	0.823	2.680	0.011	-1.950	0.071	Uncorrelated
	Total BV/TV	0	-1.850	-3.310	-1.030	0.032	1.800	0.536	Uncorrelated
	Ct.Th	1	-2.230	-4.000	-1.250	0.040	2.230	0.493	Uncorrelated
Gorilla	BV/TV	0	-1.010	-1.720	-0.597	0.064	0.859	0.342	Uncorrelated
	DA	0	0.712	0.418	1.210	0.050	-1.450	0.403	Uncorrelated
	Tb.Th	1	0.959	0.678	1.360	0.618	-1.650	**<0.001**	**Isometry**
	Tb.N	0	-1.220	-1.670	-0.895	0.693	1.490	**<0.001**	**Negative**
	Tb.Sp	1	1.450	1.020	2.070	0.602	-1.940	**<0.001**	**Positive**
	Total BV/TV	0	-0.833	-1.430	-0.484	0.011	0.802	0.698	Uncorrelated
	Ct.Th	1	1.670	1.080	2.560	0.402	-2.280	**0.008**	**Positive**
Pongo	BV/TV	0	2.570	1.410	4.690	0.077	-3.320	0.358	Uncorrelated

	DA	0	-1.180	-2.010	-0.690	0.291	0.761	0.057	Uncorrelated
	Tb.Th	1	1.690	1.010	2.850	0.328	**-2.440**	**0.040**	**Positive**
	Tb.N	0	-1.030	-1.880	-0.567	0.079	1.180	0.351	Uncorrelated
	Tb.Sp	1	1.330	0.711	2.470	<0.001	-1.660	0.980	Uncorrelated
	Total BV/TV	0	2.040	1.160	3.580	0.203	-2.560	0.123	Uncorrelated
	Ct.Th	1	3.250	2.000	5.280	0.425	**-3.940**	**0.015**	**Positive**

1130

Figure legends

Figure 1. CT-derived surface models of a left capitate from each genus showing variation in external morphology. Capitates have been scaled to relative size. Rows: 1) Capitates are oriented dorso-radially 2) Capitates are oriented dorsally. Columns: A) *Homo sapiens* (DCW_AM_10_0_182), B) *Pan troglodytes* (SMF_4104), C) *Gorilla gorilla* (ZMB_83587), D) *Pongo pygmaeus* (ZMB_6948). Numbers representing anatomical features: '1' MC2 articulation, '2' Dorsal ridge, '3' trapezoid articulation, '4' radial-palmar expansion of the proximal capitate, '5' Mc3 styloid process articulation, '6' waisted mid-capitate.

Figure 2. Images showing the morphological filters applied in medtool 4.3 for the whole-bone analysis. A) Original microCT of a *Homo sapiens* capitate, B) MicroCT scan after MIA-clustering segmentation, C) Cortical thickness image stack, allowing analysis of the cortex only, D) Trabecular bone image stack, allowing analysis of the trabeculae (white) only, E) Combined mask overlay, identifying cortical (lightest grey), trabecular (mid-grey) and air (darkest grey internally and black externally) voxels, F) Sampling sphere (blue) moving across each node of the overlaid 3D grid (red) measuring bone parameters in the trabecular bone image stack.

Figure 3. Three cross-sections from the four study genera showing internal bone patterning. A) Y-Z dimension, radial-ulnar cross-section, slice taken from mid-section of bone. Distal is up; dorsal is left. B) X-Y dimension, proximal-distal cross-section, slice taken from proximal mid-capitate. Dorsal is up; radial is left. C) X-Z dimension, dorsal-palmar cross-section, slice taken from midsection of bone. Ulnar is up; proximal is left. D) Surface models of each bone showing the location of cross-section A, B and C. The red dotted line indicates where capitates were partitioned into a distal and proximal VOI. Capitates are not to scale. Left capitates have been mirrored.

Figure 4. Split violin plots showing the distribution of trabecular results in the proximal and distal VOI of each genus. Images are generated using *ggplot2* in *R* (v. 1.2.1335) and utilize the default (Gaussian) kernel density estimation. Colored contours indicate the density of results across the data range. A) Trabecular bone volume to total volume; B) Degree of anisotropy; C) trabecular thickness; D) trabecular number; E) trabecular separation. Outliers are identified with ● and represent values 1.5 times above the fourth or below the first interquartile range. For all plots: significant pairwise comparisons are indicated by the square brackets for the distal VOI tests (top of graph) and proximal VOI tests (bottom of graph), * = $p \leq 0.05$; ** = $p \leq 0.001$.

Figure 5. Boxplots of the five trabecular ratios for each genus as well as results for the intraspecific Wilcoxon signed-rank test and interspecific pairwise rank-sum tests. A) Ratio of distal to proximal

trabecular BV/TV; B) Ratio of distal to proximal DA; C) Ratio of distal to proximal Tb.Th.; D) Ratio of distal to proximal Tb.N (green) and Tb.Sp (orange). For all figures: Values above the dotted line (ratio = 1) indicate greater trabecular variable in the distal capitate. Significant pairwise comparisons of the ratios are indicated by the square brackets. For D, the top brackets indicate the tests for Tb.N and the bottom brackets indicate those for Tb.Sp. * = $p \leq 0.05$; ** = $p \leq 0.001$. Significant intraspecific Wilcoxon signed-rank tests between the proximal and distal means are represented by the ◆ symbol thus indicate whether the difference between the mean distal and proximal trabecular variable was significantly different. ◆ = $p \leq 0.05$; ◆ ◆ = $p \leq 0.001$.

Figure 6. A-B: Split violin plots showing the distribution of total BV/TV (A) and Ct.Th (B) results in the proximal and distal VOI of each genus. Images are generated using *ggplot2* in *R* (v. 1.2.1335) and utilize the default (Gaussian) kernel density estimation. Colored contours indicate the density of results across the data range. Outliers are identified with ● and represent values 1.5 times above the fourth or below the first interquartile range. Significant pairwise comparisons are indicated by the square brackets for the distal tests (top of graph) and proximal tests (bottom of graph), * = $p \leq 0.05$; ** = $p \leq 0.001$. C-D: Boxplots showing the distribution of the distal to proximal ratios of the total BV/TV (C) and Ct.Th (D) of each genus. Boxplots also show the results of the intraspecific Wilcoxon signed-rank test and interspecific pairwise rank-sum tests. Values above the dotted line (ratio = 1) indicate greater cortical variable in the distal capitate. Significant pairwise comparisons of the ratios are indicated by the square brackets, * = $p \leq 0.05$; ** = $p \leq 0.001$. Significant intraspecific Wilcoxon signed-rank tests between the proximal and distal means are represented by the ◆ symbol thus indicate whether the difference between the mean distal and proximal trabecular variable was significantly different. ◆ = $p \leq 0.05$; ◆ ◆ = $p \leq 0.001$.

Figure 7. Cross-sections from representative individuals of each genus showing relative trabeculae and cortex thickness across the capitate. A) Y-Z dimension, radio-ulnar cross-section. Distal is up; dorsal is left. B) X-Z dimension, dorsal-palmar cross-section. Ulnar is up; distal is left. C) X-Y dimension, proximal-distal cross-section. Cross-section taken at the proximal mid-capitate. Dorsal is up; radial is left. D) X-Y dimension, proximal-distal cross-section. Cross-section taken at the distal capitate. Dorsal is up; ulnar is left. E) Shows the positions of cross-sections A-D on a *Pan* specimen. Left capitates have been mirrored. Capitates not to scale.

Cortical and trabecular bone structure of the hominoid capitate

Emma E. Bird, Tracy L. Kivell, and Matthew M. Skinner.

Supplementary Table 1. Downloadable excel file recording specimen information and individual para
= Max Planck Institute for Evolutionary Anthropology Primatology, Tai Collection; MRAC = Royal Mus
Museum, Frankfurt; UNI_FL = University of Florence; ZMB = the Natural History Museum, Berlin; ZSM

Specimen	Taxon	Sex	Side	Resolution	Whole Trabecular
DCW_AM_10_0_182	Homo sapiens	Unknown	Right	0.0314	0.2873
DCW_AM_10_0_183	Homo sapiens	Unknown	Right	0.0315	0.3465
DCW_AM_3_0_1	Homo sapiens	Unknown	Left	0.0345	0.1679
DCW_AM_3_0_2	Homo sapiens	Unknown	Left	0.0294	0.1884
DCW_OC_1_0_26	Homo sapiens	Unknown	Right	0.0264	0.2237
DCW_OC_31_0_1	Homo sapiens	Unknown	Left	0.0302	0.2214
DCW_OC_31_0_2	Homo sapiens	Unknown	Left	0.0306	0.2329
INDEN_113	Homo sapiens	Male	Right	0.0251	0.3483
INDEN_118	Homo sapiens	Female	Right	0.0251	0.3401
INDEN_243	Homo sapiens	Male	Left	0.0301	0.3333
INDEN_311	Homo sapiens	Male	Left	0.0301	0.3424
INDEN_323	Homo sapiens	Unknown	Right	0.0301	0.3260
INDEN_340	Homo sapiens	Unknown	Left	0.0301	0.2618
INDEN_91	Homo sapiens	Male	Right	0.0301	0.3482
MPI_TC_11778	Pan troglodytes	Female	Right	0.0251	0.3660
MPI_TC_11781	Pan troglodytes	Male	Right	0.0302	0.3598
MPI_TC_11789	Pan troglodytes	Male	Left	0.0302	0.3533
MPI_TC_14996	Pan troglodytes	Female	Left	0.0302	0.3004
MRAC_15293	Pan paniscus	Female	Right	0.0302	0.3292
MRAC_15294	Pan paniscus	Male	Left	0.0302	0.4011
MRAC_27696	Pan paniscus	Male	Right	0.0302	0.3146
MRAC_27698	Pan paniscus	Female	Left	0.0302	0.4496
MRAC_29042	Pan paniscus	Female	Left	0.0302	0.4306
MRAC_29044	Pan paniscus	Male	Right	0.0400	0.3807
MRAC_29045	Pan paniscus	Female	Right	0.0309	0.3368
MRAC_29052	Pan paniscus	Male	Right	0.0340	0.3731
NGB_89_SK15_1247	Homo sapiens	Unknown	Left	0.0300	0.3149
NHMW_J_2	Homo sapiens	Male	Right	0.0300	0.2325
NHMW_J3	Homo sapiens	Unknown	Left	0.0301	0.1979
NHMW_K_13_3	Homo sapiens	Male	Right	0.0300	0.3173
NHMW_K_41_2	Homo sapiens	Unknown	Left	0.0302	0.2768
NHMW_K18_2	Homo sapiens	Female	Right	0.0301	0.3026
NHMW_K24_2	Homo sapiens	Female	Right	0.0202	0.2053
NHMW_K5_II	Homo sapiens	Male	Right	0.0301	0.3511
NHMW_K78_2	Homo sapiens	Female	Right	0.0319	0.2524

NMNH_267325	Pongo abelii	Male	Left	0.0318	0.3774
PC_CAMI_230	Gorilla gorilla	Male	Left	0.0344	0.5094
PC_MER_138	Gorilla gorilla	Female	Left	0.0353	0.3770
PC_MER_174	Gorilla gorilla	Male	Right	0.0282	0.4488
PC_MER_264	Gorilla gorilla	Male	Right	0.0369	0.4212
PC_MER_300	Gorilla gorilla	Female	Right	0.0363	0.4253
PC_MER_372	Gorilla gorilla	Male	Right	0.0352	0.4536
PC_MER_696	Gorilla gorilla	Female	Right	0.0308	0.4554
PC_MER_856	Gorilla gorilla	Female	Left	0.0341	0.4760
PC_MER_879	Gorilla gorilla	Male	Left	0.0319	0.3780
PC_MER_95	Gorilla gorilla	Female	Left	0.0318	0.3646
PC_MERI_29	Gorilla gorilla	Female	Left	0.0301	0.4829
SMF_24510	Pongo pygmaeus	Female	Right	0.0318	0.2519
SMF_4104	Pan troglodytes	Unknown	Left	0.0316	0.3161
SMF_63976	Gorilla beringei	Unknown	Left	0.0301	0.4440
SMF_6999	Pongo abelii	Female	Right	0.0294	0.2078
SMF_84218	Pongo pygmaeus	Female	Left	0.0302	0.3625
UNI_FL_3127	Homo sapiens	Male	Left	0.0302	0.2525
UNI_FL_4865	Homo sapiens	Male	Right	0.0302	0.1955
UNI_FL_4887	Homo sapiens	Female	Left	0.0301	0.1737
ZMB_11647	Pongo pygmaeus	Unknown	Left	0.0481	0.3047
ZMB_18516	Gorilla gorilla	Unknown	Right	0.0302	0.3397
ZMB_6947	Pongo pygmaeus	Male	Left	0.0318	0.3347
ZMB_6948	Pongo pygmaeus	Female	Left	0.0321	0.2973
ZMB_83530	Gorilla gorilla	Male	Right	0.0302	0.2915
ZMB_83545	Gorilla gorilla	Male	Right	0.0301	0.3932
ZMB_83587	Gorilla gorilla	Female	Left	0.0409	0.3655
ZSM_1907_0622	Pongo pygmaeus	Unknown	Right	0.0293	0.3367
ZSM_1907_0629b	Pongo pygmaeus	Male	Right	0.0284	0.4706
ZSM_1907_0633b	Pongo pygmaeus	Female	Right	0.0293	0.4547
ZSM_1907_0660	Pongo pygmaeus	Female	Right	0.0284	0.3291
ZSM_1909_0801	Pongo pygmaeus	Male	Right	0.0343	0.3839
ZSM_AP_122	Pan troglodytes	Male	Right	0.0364	0.3958
ZSM_AP-120	Pongo pygmaeus	Male	Left	0.0284	0.3846

ameter values. The specimen column records the curatorial institutions as abbreviations; DCV
seum for Central Africa Tervuren; NGB = University of Kent; NHMW = Natural History Museur
M = Bavarian State Collection Zoology.

Proximal Trabecu	Distal Trabecu	Whole DA	Proximal DA	Distal DA	Whole Tb.Th
0.3145	0.2803	0.3047	0.3156	0.3019	0.1903
0.3979	0.3315	0.3145	0.3340	0.3088	0.2467
0.2304	0.1494	0.3681	0.3951	0.3601	0.2288
0.2164	0.1832	0.3185	0.3658	0.3098	0.1827
0.2397	0.2166	0.2474	0.2592	0.2423	0.1870
0.2311	0.2178	0.2892	0.3193	0.2780	0.2013
0.2890	0.2181	0.2527	0.2988	0.2406	0.2026
0.3705	0.3364	0.2860	0.3086	0.2739	0.2740
0.3526	0.3339	0.2645	0.2843	0.2546	0.3248
0.3654	0.3196	0.2837	0.3310	0.2635	0.2701
0.3721	0.3303	0.2906	0.3008	0.2865	0.3005
0.3573	0.3156	0.3058	0.3192	0.3014	0.2367
0.2888	0.2490	0.2773	0.2915	0.2706	0.2326
0.3726	0.3377	0.2997	0.3055	0.2973	0.2518
0.3891	0.3467	0.2525	0.2440	0.2596	0.2139
0.4003	0.3322	0.2735	0.2532	0.2873	0.2690
0.3809	0.3320	0.2550	0.2038	0.2946	0.2372
0.3078	0.2965	0.2881	0.2817	0.3013	0.2070
0.3599	0.3112	0.2675	0.2660	0.2684	0.2342
0.4242	0.3839	0.2367	0.2185	0.2503	0.2874
0.3245	0.3073	0.2570	0.2627	0.2528	0.2252
0.4652	0.4367	0.2567	0.2528	0.2601	0.2841
0.4553	0.4140	0.2636	0.2646	0.2629	0.2690
0.3902	0.3707	0.2367	0.2116	0.2319	0.2520
0.3453	0.3302	0.2618	0.2555	0.2668	0.2212
0.4004	0.3570	0.2777	0.2907	0.2699	0.2347
0.3194	0.3134	0.2438	0.2781	0.2329	0.2189
0.2606	0.2217	0.2951	0.2924	0.2971	0.2081
0.2352	0.1821	0.3281	0.3463	0.3186	0.1729
0.3176	0.3204	0.2750	0.3254	0.2545	0.3270
0.3137	0.2693	0.2606	0.2333	0.2667	0.2487
0.3178	0.2989	0.2365	0.2185	0.2385	0.2435
0.2152	0.2015	0.2722	0.3003	0.2530	0.2072
0.4291	0.3586	0.2553	0.2335	0.2574	0.2406
0.2242	0.2248	0.2470	0.3201	0.2234	0.2031

0.3693	0.3828	0.2527	0.2675	0.2428	0.3066
0.5434	0.4765	0.2543	0.2482	0.2602	0.3678
0.4158	0.3558	0.2798	0.2507	0.2958	0.2947
0.4875	0.4242	0.2432	0.1936	0.2748	0.2898
0.4692	0.3885	0.2756	0.2367	0.3021	0.4084
0.4620	0.4046	0.2456	0.2297	0.2516	0.3579
0.4826	0.4307	0.2529	0.2305	0.2706	0.4110
0.4709	0.4420	0.2429	0.2077	0.2733	0.3162
0.5182	0.4527	0.2700	0.2366	0.2885	0.3534
0.4105	0.3618	0.3323	0.2968	0.3499	0.3623
0.3757	0.3549	0.2415	0.2479	0.2359	0.3319
0.4774	0.4873	0.3144	0.3136	0.3152	0.3057
0.2274	0.2711	0.2601	0.2901	0.2500	0.2671
0.3428	0.3009	0.2029	0.1713	0.2209	0.2515
0.4521	0.4426	0.2361	0.2306	0.2553	0.3468
0.1800	0.2162	0.2894	0.2846	0.2909	0.1944
0.3667	0.3587	0.3266	0.3445	0.3093	0.2712
0.2724	0.2482	0.3221	0.3628	0.3024	0.1703
0.2230	0.1876	0.3086	0.3228	0.3045	0.2088
0.2010	0.1668	0.3264	0.3567	0.3105	0.1785
0.3085	0.3059	0.2548	0.2809	0.2439	0.2898
0.3546	0.3289	0.2643	0.2387	0.2829	0.2376
0.4355	0.3108	0.2987	0.2737	0.3060	0.2860
0.3176	0.2839	0.3108	0.3403	0.2902	0.2784
0.3011	0.2898	0.3081	0.3178	0.3065	0.3841
0.4234	0.3753	0.2442	0.2267	0.2546	0.3581
0.3915	0.3450	0.2587	0.2282	0.2828	0.3256
0.3688	0.3228	0.3213	0.3051	0.3240	0.2454
0.5289	0.4391	0.2903	0.3074	0.2821	0.3541
0.5254	0.4248	0.2735	0.2804	0.2838	0.3159
0.3119	0.3444	0.3286	0.3946	0.3029	0.2392
0.3980	0.3782	0.2447	0.2563	0.2401	0.2608
0.4149	0.3749	0.2969	0.2771	0.3188	0.2586
0.4546	0.3484	0.2983	0.3616	0.2657	0.2559

N = The Duckworth Collection, University of Cambridge; INDEN = Georg-August-University Goettingen, Ant
m Vienna; NMNH = National Museum Natural History Smithsonian; PC = Powell-Cotton Museum; SMF = Se

Proximal Tb.Th	Distal Tb.Th	Whole Tb.N	Proximal Tb.N	Distal Tb.N	Whole Tb.Sp
0.1846	0.1920	1.4483	1.6340	1.4081	0.5002
0.2553	0.2438	1.2003	1.3167	1.1748	0.5864
0.2574	0.2160	0.7891	0.8974	0.7687	1.0385
0.1863	0.1819	1.1019	1.2615	1.0772	0.7249
0.1879	0.1863	0.9849	1.0194	0.9759	0.8284
0.2054	0.1998	1.1256	1.1209	1.1273	0.6871
0.2126	0.1993	1.2257	1.3282	1.2050	0.6132
0.2782	0.2717	1.1200	1.1320	1.1151	0.6189
0.3322	0.3212	0.9757	0.9723	0.9773	0.7000
0.2821	0.2644	1.1612	1.1547	1.1653	0.5911
0.3045	0.2988	1.0698	1.1033	1.0580	0.6343
0.2393	0.2358	1.2971	1.3523	1.2816	0.5343
0.2347	0.2315	1.1173	1.1916	1.0875	0.6624
0.2473	0.2539	1.3095	1.4007	1.2762	0.5118
0.2241	0.2048	1.5312	1.4957	1.5631	0.4392
0.2976	0.2460	1.1528	1.0953	1.1993	0.5985
0.2557	0.2215	1.3327	1.2642	1.3904	0.5132
0.2111	0.2081	1.2014	1.2431	1.2628	0.6253
0.2501	0.2238	1.2215	1.1447	1.2706	0.5845
0.2974	0.2794	1.1602	1.1133	1.1973	0.5745
0.2285	0.2229	1.3430	1.2770	1.3921	0.5194
0.2942	0.2752	1.3009	1.2601	1.3370	0.4846
0.2833	0.2589	1.3372	1.2935	1.3680	0.4789
0.2534	0.2505	1.3207	1.2941	1.3488	0.5052
0.2233	0.2196	1.3604	1.3582	1.3627	0.5139
0.2510	0.2233	1.3351	1.2491	1.3958	0.5143
0.2219	0.2179	1.3860	1.3774	1.3888	0.5027
0.2084	0.2119	1.1091	1.2120	1.0529	0.6935
0.1861	0.1698	1.2094	1.2320	1.1905	0.6540
0.3265	0.3371	0.8599	0.8850	0.8409	0.8359
0.2554	0.2539	1.1441	1.2530	1.1041	0.6253
0.2298	0.2558	1.0568	1.2555	0.9831	0.7027
0.1993	0.2141	1.0839	1.1649	1.0433	0.7154
0.2510	0.2577	1.3788	1.5304	1.3161	0.4846
0.1677	0.2000	1.3532	1.5525	1.3246	0.5359

0.2874	0.3194	1.0659	1.1215	1.0315	0.6315
0.3810	0.3536	1.0076	1.0568	0.9742	0.6247
0.2983	0.2927	0.9936	1.0946	0.9504	0.7117
0.3056	0.2785	1.2493	1.2928	1.2300	0.5107
0.4320	0.3896	0.7752	0.8243	0.7524	0.8816
0.3689	0.3557	0.9626	0.9736	0.9452	0.6810
0.4265	0.3975	0.8516	0.8703	0.8406	0.7632
0.3305	0.3030	1.0994	1.1270	1.0794	0.5934
0.3555	0.3524	0.9928	1.0753	0.9562	0.6538
0.3647	0.3612	0.8120	0.8565	0.7935	0.8692
0.3294	0.3344	0.8838	0.9333	0.8464	0.7995
0.3140	0.2997	1.1178	1.0182	1.2139	0.5889
0.2379	0.2875	0.9909	1.0322	0.9598	0.7421
0.2641	0.2429	1.1863	1.1644	1.2014	0.5914
0.3647	0.3778	1.0437	1.0367	0.9375	0.6113
0.1666	0.2013	1.1636	1.3100	1.1265	0.6649
0.2665	0.2804	1.1542	1.1659	1.1328	0.5952
0.1757	0.1721	1.4796	1.5026	1.4584	0.5055
0.2087	0.2089	1.0047	1.0539	0.9924	0.7865
0.1764	0.1814	1.2533	1.3237	1.2265	0.6195
0.2785	0.3025	1.0292	1.0855	0.9908	0.6817
0.2323	0.2419	1.2793	1.3352	1.2446	0.5441
0.2773	0.2921	0.9573	1.2279	0.9062	0.7585
0.2637	0.2964	0.9134	1.0768	0.8254	0.8164
0.3860	0.3829	0.6332	0.6480	0.6241	1.1953
0.3503	0.3637	0.8957	1.0137	0.8443	0.7583
0.3382	0.3099	0.9748	0.9512	1.0030	0.7003
0.2439	0.2473	1.1840	1.3489	1.1344	0.5992
0.3625	0.3571	1.0402	1.1066	1.0027	0.6073
0.3347	0.3127	1.1339	1.2276	1.0701	0.5660
0.2127	0.2546	1.1801	1.2879	1.1392	0.6081
0.2575	0.2623	1.2092	1.2988	1.1778	0.5662
0.2714	0.2433	1.3084	1.2676	1.3576	0.5057
0.2627	0.2514	1.1202	1.2946	1.0608	0.6369

:hropology Collection; MPI_TC
:nckenberg Natural History

Proximal Tb.Sp	Distal Tb.Sp	Proximal Total BV/TV	Distal Total BV/TV	Whole Ct.Th
0.4274	0.5182	0.3909	0.3652	0.2379
0.5042	0.6074	0.4511	0.4154	0.2973
0.8569	1.0849	0.3099	0.2336	0.3005
0.6064	0.7464	0.2888	0.2465	0.1969
0.7930	0.8384	0.3123	0.3023	0.2326
0.6868	0.6872	0.3245	0.3313	0.2663
0.5403	0.6306	0.4030	0.3623	0.2952
0.6052	0.6251	0.4322	0.4212	0.3413
0.6962	0.7020	0.4509	0.4359	0.3671
0.5839	0.5937	0.4595	0.4219	0.3751
0.6019	0.6464	0.4640	0.4328	0.3960
0.5002	0.5445	0.4542	0.4108	0.3142
0.6045	0.6881	0.3698	0.3445	0.2804
0.4666	0.5296	0.4545	0.4450	0.3618
0.4444	0.4349	0.5010	0.5622	0.4409
0.6154	0.5878	0.5569	0.5465	0.5448
0.5353	0.4977	0.5393	0.5629	0.5321
0.5934	0.5838	0.3870	0.4510	0.4434
0.6234	0.5632	0.4287	0.4454	0.4408
0.6008	0.5558	0.5234	0.6343	0.6250
0.5546	0.4954	0.4029	0.4791	0.5457
0.4993	0.4727	0.6253	0.6836	0.6767
0.4899	0.4721	0.5561	0.6038	0.5438
0.5193	0.4909	0.5491	0.6426	0.5760
0.5130	0.5143	0.4527	0.5406	0.6002
0.5496	0.4932	0.5170	0.5549	0.4229
0.5041	0.5021	0.4135	0.4085	0.2811
0.6167	0.7378	0.3315	0.3218	0.3280
0.6256	0.6702	0.3070	0.2523	0.2202
0.8034	0.8522	0.4017	0.4522	0.3881
0.5426	0.6518	0.3977	0.3791	0.2959
0.5667	0.7613	0.4088	0.4138	0.3298
0.6591	0.7445	0.2874	0.2929	0.2590
0.4025	0.5021	0.5091	0.4938	0.3821
0.4765	0.5550	0.3029	0.3137	0.2974

0.6043	0.6501	0.4447	0.5914	0.4403
0.5652	0.6729	0.6797	0.7405	0.7061
0.6153	0.7595	0.4955	0.5378	0.4103
0.4679	0.5345	0.5785	0.6519	0.4158
0.7812	0.9395	0.6040	0.6749	0.7450
0.6582	0.7023	0.5738	0.6253	0.6216
0.7225	0.7921	0.5728	0.6807	0.6200
0.5569	0.6235	0.5461	0.6256	0.3971
0.5744	0.6934	0.6643	0.7239	0.5640
0.8027	0.8990	0.5343	0.5686	0.6787
0.7421	0.8471	0.4786	0.5782	0.5596
0.6682	0.5241	0.6020	0.7127	0.5470
0.7309	0.7543	0.3247	0.4994	0.6061
0.5947	0.5895	0.4657	0.4863	0.4326
0.5998	0.6888	0.5489	0.6635	0.7222
0.5968	0.6864	0.2477	0.3483	0.3133
0.5913	0.6023	0.4352	0.5580	0.4588
0.4899	0.5136	0.3723	0.3509	0.2707
0.7402	0.7988	0.2920	0.2682	0.2666
0.5791	0.6340	0.2697	0.2441	0.2545
0.6427	0.7068	0.3978	0.5498	0.6941
0.5167	0.5615	0.4302	0.5173	0.4858
0.5371	0.8114	0.5608	0.5265	0.4781
0.6650	0.9152	0.3839	0.4902	0.4672
1.1571	1.2195	0.4177	0.4851	0.6852
0.6361	0.8207	0.5256	0.6716	0.9716
0.7131	0.6871	0.5020	0.6047	0.5475
0.4974	0.6342	0.4473	0.4599	0.3155
0.5411	0.6402	0.6130	0.6697	0.7569
0.4798	0.6218	0.6113	0.6460	0.5531
0.5637	0.6232	0.4150	0.5196	0.3788
0.5124	0.5868	0.4868	0.5408	0.3744
0.5175	0.4934	0.5071	0.6022	0.5143
0.5097	0.6913	0.5308	0.5548	0.3641

Proximal Ct.Th	Distal Ct.Th	Size (mm3)
0.2176	0.2424	2862
0.2318	0.3105	2802
0.2734	0.3084	3522
0.2009	0.1959	2048
0.2207	0.2415	1902
0.2746	0.2639	1900
0.3081	0.2923	2284
0.2597	0.3722	2833
0.3327	0.3810	2258
0.3583	0.3823	3327
0.3861	0.3999	3606
0.3124	0.3151	2623
0.2766	0.2822	3305
0.3257	0.3736	3517
0.3323	0.4774	2524
0.5005	0.5662	3634
0.4174	0.5860	2854
0.3316	0.4950	2886
0.3171	0.4739	1825
0.4249	0.6625	1670
0.3014	0.6038	2362
0.5205	0.7484	1941
0.3635	0.6007	2708
0.4145	0.6455	2072
0.3616	0.6680	2418
0.3271	0.4535	2144
0.2680	0.2856	2277
0.2767	0.3517	2495
0.2420	0.2233	2531
0.2870	0.4214	2854
0.2690	0.3113	1558
0.3230	0.3396	2044
0.2499	0.2697	1692
0.3428	0.4201	2892
0.2247	0.2806	1714

0.2780	0.4640	2974
0.5079	0.7867	5584
0.2928	0.4343	3888
0.3461	0.4291	3200
0.4740	0.8151	7341
0.4364	0.6797	4169
0.3820	0.6676	7459
0.3170	0.4179	4212
0.4700	0.5861	3277
0.5298	0.7179	10200
0.4013	0.6016	4658
0.4014	0.5875	2638
0.3179	0.6832	2424
0.3543	0.4652	2426
0.4485	0.8685	6882
0.1839	0.3294	1580
0.2650	0.5221	1957
0.2677	0.2796	1190
0.2334	0.2754	2746
0.2154	0.2675	2100
0.3228	0.7668	3078
0.2381	0.5407	2452
0.3402	0.5069	1756
0.2499	0.5188	1814.2
0.5265	0.7313	9888
0.3744	1.0518	5988
0.4354	0.5907	4187
0.2426	0.3375	1452
0.3473	0.8536	3182
0.3512	0.6188	1643
0.3037	0.4107	1914
0.2766	0.3928	2151
0.3390	0.5687	2397
0.2713	0.3817	2299